REPORT NO. GDCA-DBG73-006
CONTRACT NAS 8-27738

DESIGN, MANUFACTURE, DEVELOPMENT, TEST, AND EVALUATION OF BORON/ALUMINUM STRUCTURAL COMPONENTS FOR SPACE SHUTTLE

VOLUME III • SHEAR BEAM COMPONENT TEST AND ANALYSIS

E. E. Spier
M. F. Miller

February 1974

Prepared Under
Contract NAS8-27738

Submitted to
National Aeronautics and Space Administration
GEORGE C. MARSHALL SPACE FLIGHT CENTER
Huntsville, Alabama

Prepared by
CONVAIR AEROSPACE DIVISION OF GENERAL DYNAMICS
San Diego, California

FOREWORD

The following final report describes work performed on NASA Contract NAS 8-27738 by the San Diego Operation, Convair Aerospace Division of General Dynamics Corporation. The work was administered by the Materials Division of the Astronautics Laboratory, George C. Marshall Space Flight Center, Huntsville, Alabama 35812. Mr. F. P. LaIacona was the NASA project officer.

The program was conducted by the Advanced Composites Group at Convair Aerospace, San Diego Operations. The authors wish to express their appreciation to the following people for their contributions that assisted in making this report possible: Mr. Felix LaIacona, the NASA COR for the program; Mr. Oliver Meredith, alternate COR (design); Messers A. Robertson and C. Maikish, principal investigators during panel fabrication at General Dynamics; Messers F. Fujimoto and R. Eckberg of General Dynamics, panel designers; Mr. J. Christian and Dr. N. R. Adsit of General Dynamics, material testing; and Messers A. Dawley, H. Mammac, B. Hancock, W. Karr, W. Gill, and O. Edwards, NASA test control personnel.

This report covers testing and subsequent analysis of the shear beam component test specimen described in Volumes I and II.

Dr. M. F. Miller
Program Manager

J. L. Christian
Deputy Program Manager

"Pages missing from available version"

NOMENCLATURE

Section	Symbol	Description
4	A_{ij}	Elastic extensional stiffness coefficient (a constant)
	A^{I}_{ij}	Inelastic extensional stiffness coefficient (varies with stress level)
	D_{ij}	Elastic flexural stiffness coefficient (a constant)
	D^{I}_{ij}	Inelastic flexural stiffness coefficient (varies with stress level)
	E	Modulus of elasticity
	E_{sec}	Secant modulus of elasticity
	E_{tan}	Tangent modulus of elasticity
	E_{t}	Tensile modulus of elasticity
	F_{tu}	Ultimate tensile strength
	F_{su}	Ultimate shear strength
	G	Shear modulus of rigidity
	G_{sec}	Secant shear modulus of rigidity
	L	Length
	R	Resultant load on spot weld
	R_x, R_y, R_s	Stress ratios for ompression in the x and y directions and shear, respectively
	a	Panel length
	b	Panel width
	m	Longitudinal half wave
	n	Transverse half wave
	t	Thickness of laminate
	ϵ_x, e_y	Normal Strains in x and y directions, respectively
	ϵ_u	Ultimate strain
	ϵ_{45}	Normal strain at 45-degree counterclockwise from x-direction

NOMENCLATURE, Contd

Section	Symbol	Description
4	ϵ_{xy}	Shearing strain in x-y plane
	η	Plasticity Factor for compressive buckling
	η_x, η_y	Plasticity Factor for secant modulus of elasticity; $(E_{sec}/E)_x$, $(E_{sec}/E)_y$, respectively
	η_s	Plasticity Factor for shear, G_{sec}/G
	θ	Term defined by Equation 7-6
	ν_{xy}	Poisson's ratio, the ratio ϵ_y/ϵ_x due to applied strain in the x-direction
	ν_{yx}	Poisson's ratio, the ratio ϵ_x/ϵ_y due to applied strain in the y-direction
	σ_x, σ_y	Normal stresses in x and y directions, respectively
	σ_{xy}	Shearing stress in x-y plane
	σ_{cr}	Corrected inelastic buckling stress
	σ_{cr}/η	Calculated elastic buckling stress
	τ_{cr}	Corrected inelastic shear buckling stress
	τ_{cr}/η_s	Calculated elastic shear buckling stress
	ϕ	Term defined by Equation 7-4

ABSTRACT

A boron/aluminum composite stiffened panel was designed and fabricated by the Convair Aerospace Division of General Dynamics and tested at NASA Marshall Space Flight Center (MSFC). The panel represents a segment of a shear-resistant Space Shuttle thrust structure. The stiffened panel is approximately square in shape with closely spaced stiffeners and is cantilevered along one side. The compression cap and stiffeners are unidirectional boron/aluminum, and the web is a ±45-degree, solution-treated, cryogenically soaked, and aged boron/aluminum laminate. The boron/aluminum design represents a 34% weight savings over an equivalent all-aluminum alloy design and a 42% weight savings over an equivalent all-titanium design. A finite element analysis of the panel was performed.

The stiffened panel was extensively strain gaged, and the testing was performed by NASA-MSFC personnel. Failure occurred along a double row of web splice spot welds at 110% of design ultimate load. Correlation of strain-gage readings with the inelastic finite element analysis was made. The inelastic approach appeared to be quite satisfactory. However, improved accuracy may be achieved in the future for such a structure by other means, such as a finite element or finite difference method where incremental loading and corresponding instantaneous inelastic stiffness coefficients would be employed.

SECTION 1

INTRODUCTION

The application of advanced composites, both resin and metal matrix, to aircraft and missile structure has become prevalent in recent years. It is clear that these high-strength, low-weight composite materials will find additional structural applications on future aerospace vehicles. Previous test articles from this and other government and industry programs (References 1-6) have demonstrated that boron/aluminum (B/Al) technology has progressed sufficiently to be considered for use on Space Shuttle. In fact partly because of the present program, B/Al, tubular struts have already been used for the Space Shuttle Orbiter baseline design.

1.1 PROGRAM OBJECTIVES

The objectives of this program were to compare the use of B/Al in Space Shuttle applications with other structural materials and to evaluate material properties, processing techniques, and fabrication characteristics to develop sufficient technology to permit application of B/Al for Space Shuttle structural components with a high degree of confidence. An additional program objective relating to repairability was later added to the program. The objective of this phase of the program was to determine a basic repair approach for metal matrix-structures and to demonstrate the applicability of this approach through actual repair and re-testing.

A significant outgrowth of this contract was the design and analysis of a B/Al shear-resistant Space Shuttle thrust structure, and the subsequent design and analysis of a representative full-thickness component test panel shown in Figure 1-1. This test panel simulates the highly loaded compression side of the shear-resistant structure.

After considerable material and small-scale development testing of parts made by various fabrication and joining techniques, the test panel was designed, analyzed, and fabricated as a cantilevered structure with a web of constant thickness (References 1 and 2).

An inelastic finite element analysis was performed to determine internal stresses and strains using a technique described later in this report. The structure was designed to be shear resistant, a NASA requirement. The high compressive strength of the unidirectional B/Al cap was not utilized because of the relatively low compressive strength of the adjoining ±45-degree heat treated B/Al laminated web. At ultimate load the maximum computed compressive stress in the B/Al cap was 545 MPa (79 ksi), while the ultimate compressive strength of the material is at least 1276 MPa (185 ksi). The maximum computed ultimate compressive stress in the B/Al web was 232 MPa (33.6 ksi), while available data shows the ultimate compressive strength to be about

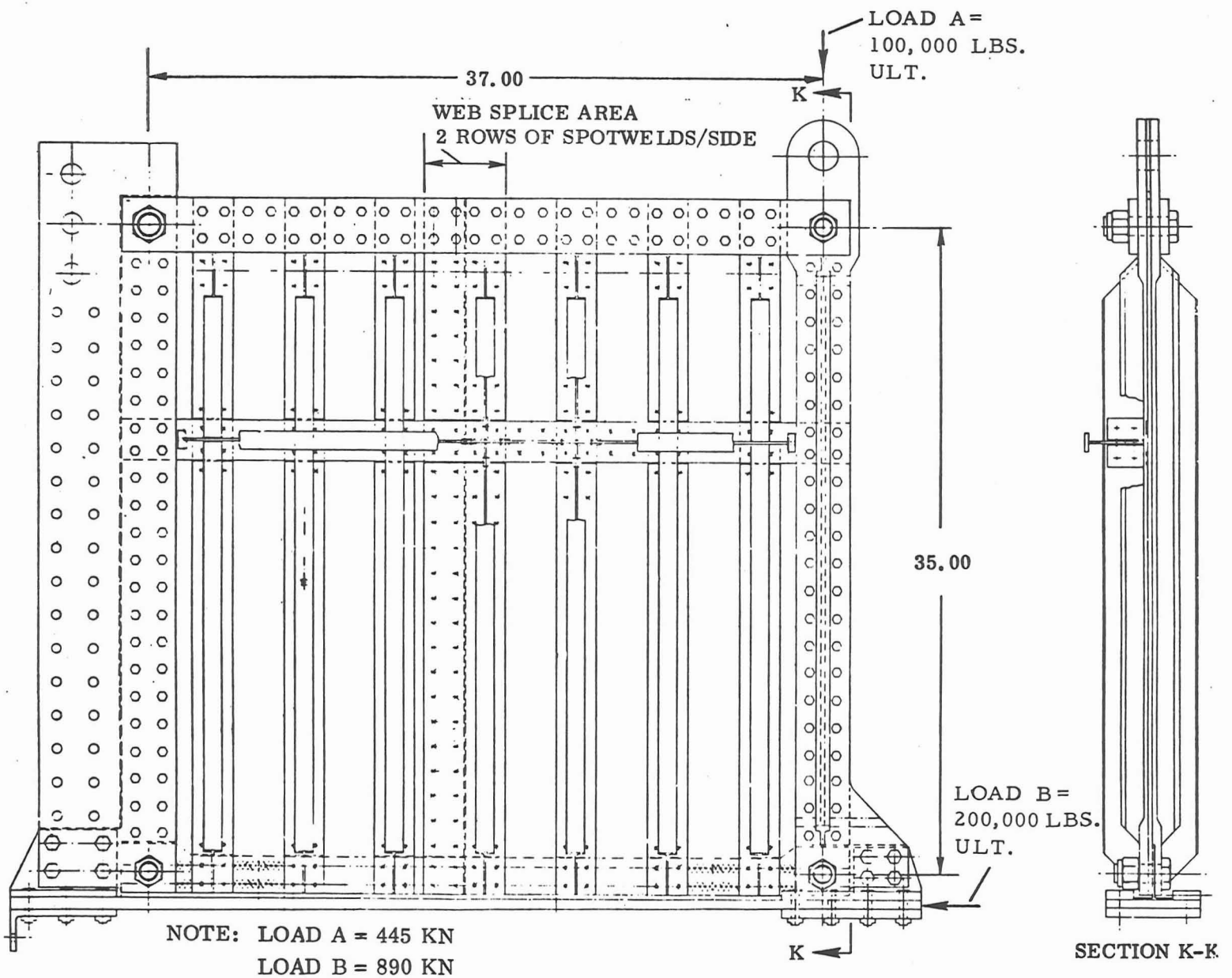

Figure 1-1. Boron/Aluminum Stiffened Panel

248 MPa (36 ksi). If incomplete tension field had been permitted to develop in the web of the structure, more efficient use could have been made of the unidirectional compression cap. In addition, fewer stiffeners would have been required. Feasibility studies (Reference 1) have indicated that the shear-resistant B/Al structure could be redesigned to accommodate an incomplete tension field design concept without affecting the overall performance of the structure.

The stiffened panel was extensively strain gaged for testing at NASA-MSFC. Failure occurred along the double row of web splice spotwelds at 110% of design ultimate load. Correlation between strain-gage data and the inelastic finite element solution was found to be satisfactory.

1.2 ORGANIZATION

This report is divided into four volumes. The first volume (Reference 1) details the design, stress analysis, and subcomponent testing of structures examined during the program. Specifically, designs are presented for 9.2 by 3.1m (30 by 10 ft) and 1.0 by 0.96m (40 by 38 in.) shear beams, a 9.2 by 3.1m (30 by 10 ft) truss, and 3.1 by 3.1m (10 by 10 ft) and 2.0 by 0.7m (80 by 29 in.) compression panels as well as several subcomponent specimens. The second volume (Reference 2) contains material characterization, process development, process and material specifications or guidelines, and manufacturing procedures used in the fabrication of component and subcomponent test articles. This third volume discusses the component testing on the full-scale shear beam test specimen, and compares the B/Al design of the component with comparable performance structures made from aluminum and titanium. Volume IV, to be published, will describe repair methods developed during this program.

1.3 NEW TECHNOLOGY

In compliance with the New Technology clause of this contract, personnel assigned to work on the program were advised, and periodically reminded, of their responsibilities in the prompt reporting of items of New Technology. In addition, reports generated as a result of the contract work were reviewed by the Program Manager as a further means of identifying items to be reported.

Response was made to all inquiries by the company-appointed New Technology Representative, and when deemed appropriate, conferences were held with the New Technology Representative to discuss new developments arising out of current work that could lead to New Technology items. The New Technology Representative has the responsibility for transmitting reportable items of New Technology to the Technology Utilization Officer, as well as the annual and final reports specified in the Clause.

The Contractor believes the performance of personnel associated with the contract has been consistent with the requirements of the New Technology clause.

SECTION 2

FABRICATION OF STIFFENED PANEL

The 1.0 by 0.96m (40 by 38 in.) boron/aluminum (B/Al) stiffened panel was fabricated to demonstrate production methods and design concepts developed on the program for a Space Shuttle shear beam thrust structure. The detailed designs and fabrication sequence for the stiffened panel are described in References 1 and 2. Fabrication procedures are briefly described below.

2.1 STIFFENERS

Twenty-one unidirectional B/Al vertical I-section stiffeners and one unidirectional B/Al horizontal I-section stiffener were fabricated for the stiffened panel. The stiffeners were fabricated using the Con Braz joining process. The combination heating and tooling module used to make the stiffeners is shown in Figure 2-1. More than 24.5m (80 ft) of stiffeners were successfully joined by this process.

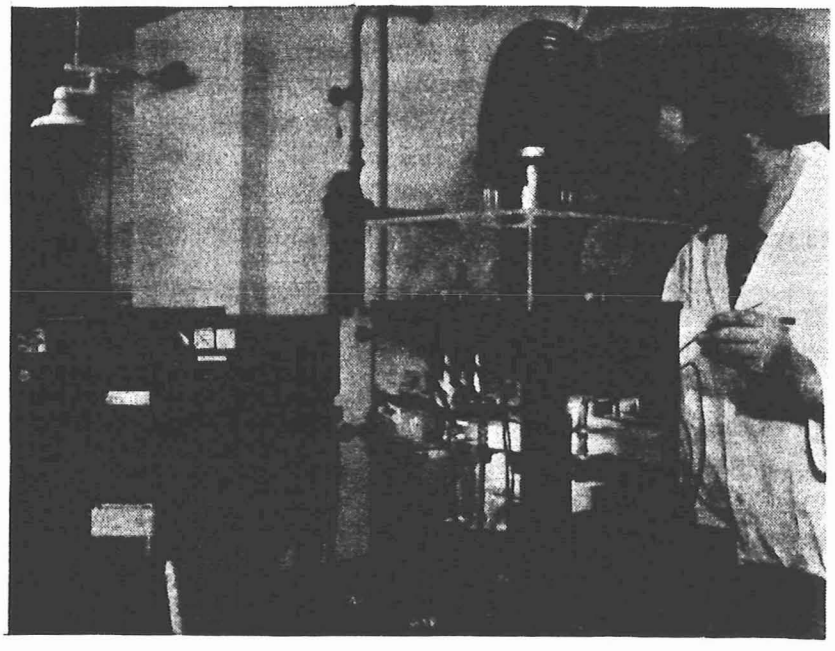

Figure 2-1. Con Braz Joining of Boron/Aluminum I-Section Stiffener (128749B)

2.2 WEB

Two diffusion-bonded, ±45-degree crossplied B/Al panels were purchased for the web of the stiffened panel, which required a splice joint. The panels were solution treated, cryogenically soaked, and then aged (ST+C+A). The solution treatment consisted of 30 minutes at 799K (980F) followed by a water quench. The cryogenic soak consisted of five minutes in liquid nitrogen, i.e., at a temperature of 77K (-320F). The panels were aged at 450K (350F) for 9 to 12 hours in an aluminum fixture (to correct warpage caused by the quench). Material test data was available only for the heat-treated material without the cryogenic soak (STA). A 10% increase in strength is expected as a result of the cryogenic soak. For expediency, the heat-treated web material was regarded as in the STA condition in the remainder of the report.

2.3 COMPRESSION CAP

The compression cap was a diffusion-bonded unidirectional B/Al part that was purchased in a tapered configuration, and required only cutting to the proper length and width prior to assembly. The width was constant, and the thickness varied from 1.7 cm (0.64 in.) to 1.2 cm (0.44 in.) over a length of 1.25m (50 in.).

The compression cap was connected to the web by a heat-treated 6Al-4V titanium T-section, which was attached to the compression cap by two rows of 30-0.64 cm (0.25 in.) diameter titanium Hi-Lok pins. The holes were drilled in the titanium part by using high-speed-steel drills and conventional machining techniques. The T-section was then used as a drill template for drilling the 0.64 cm (0.25 in.) diameter holes in the B/Al cap with diamond impregnated core drills on a rotary ultrasonic machine.

2.4 STIFFENED-PANEL WELD ASSEMBLY

The leg of the titanium T-section was attached to the B/Al web by resistance spot diffusion joining that was overlapping along two rows. The remaining B/Al composite parts were assembled by resistance spotwelding, resistance spot diffusion joining, or a combination of the two processes. A total of eight weld schedules was used during assembly. The stiffened panel is shown being welded in Figure 2-2.

2.5 FINAL ASSEMBLY OF STIFFENED PANEL

Following assembly of the stiffeners, the web, and the compression cap subassemblies, the stiffened panel was drilled and assembled in the steel test fixture, and the shear clips (that tie the vertical and horizontal stiffeners together) were installed.

Attachment of the AISI 4340 steel parts (tension cap and edge members) to the B/Al parts of the stiffened panel required the drilling of 142 holes around the periphery of the panel and 24 holes in the ends of the compression cap. All holes were drilled using the rotary ultrasonic drilling machine with diamond impregnated core drills. The

AISI 4340 steel parts were used as drill templates to ensure correct location of the holes and alignment with the steel parts in final assembly. Figure 2-3 shows the ultrasonic machine mounted on the Induma mill during drilling of the stiffened panel.

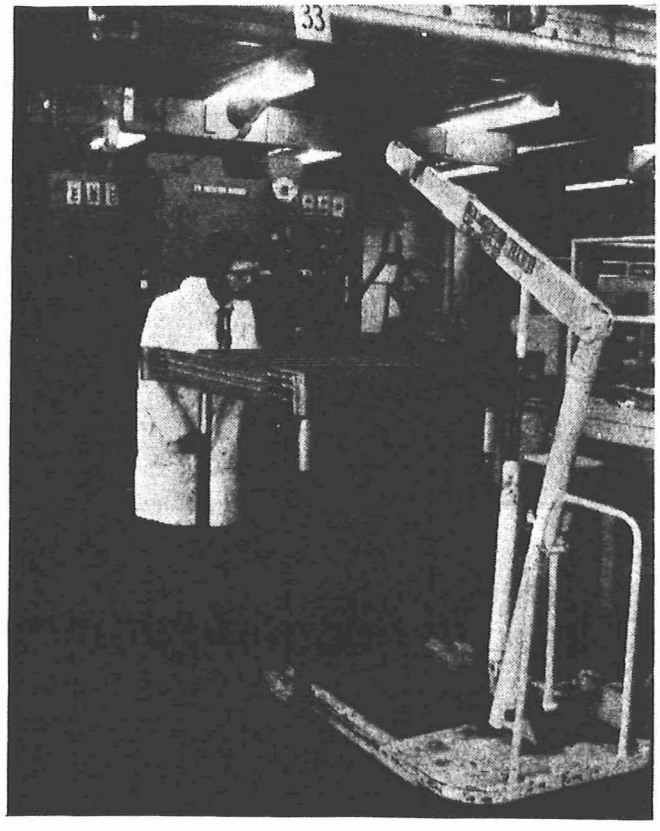

Figure 2-2. Stiffened Panel Welding Setup (127478B)

The 2024-T6 aluminum shear clips that tie the 0.17 cm (0.068 in.) thick vertical B/Al stiffeners to the 0.28 cm (0.109 in.) thick web of the horizontal stiffener were attached by titanium Hi-Lok mechanical fasteners. The holes for the fasteners were punched in the stiffeners. Figure 2-4 shows the hole punching tool being used on a stiffener. To maintain a hole tolerance of +0.05mm, -0.00mm, (+0.002 in., -0.000 in.) an additional reaming operation with a diamond-plated twist drill was performed.

The completed shear beam component stiffened panel, prior to testing, is shown in Figures 2-5 and 2-6.

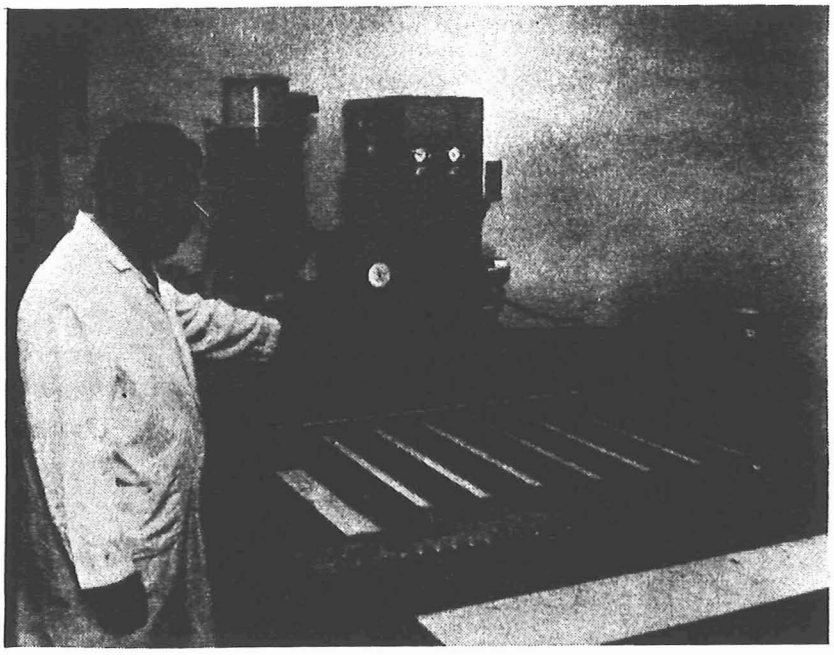

Figure 2-3. Final Drilling of the Stiffened Panel (128748B)

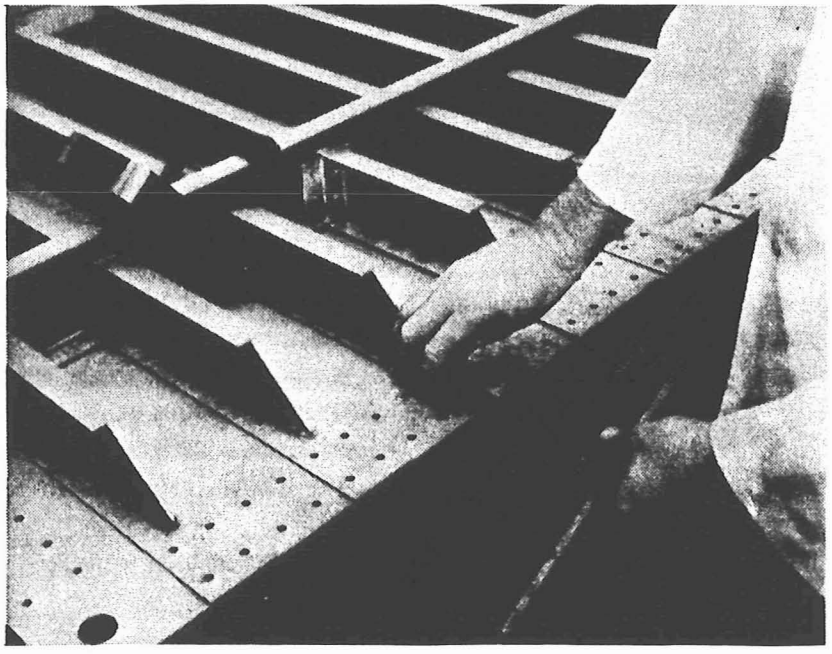

Figure 2-4. Punching Hole in B/Al Stiffeners During Assembly of Shear Clips (129427B)

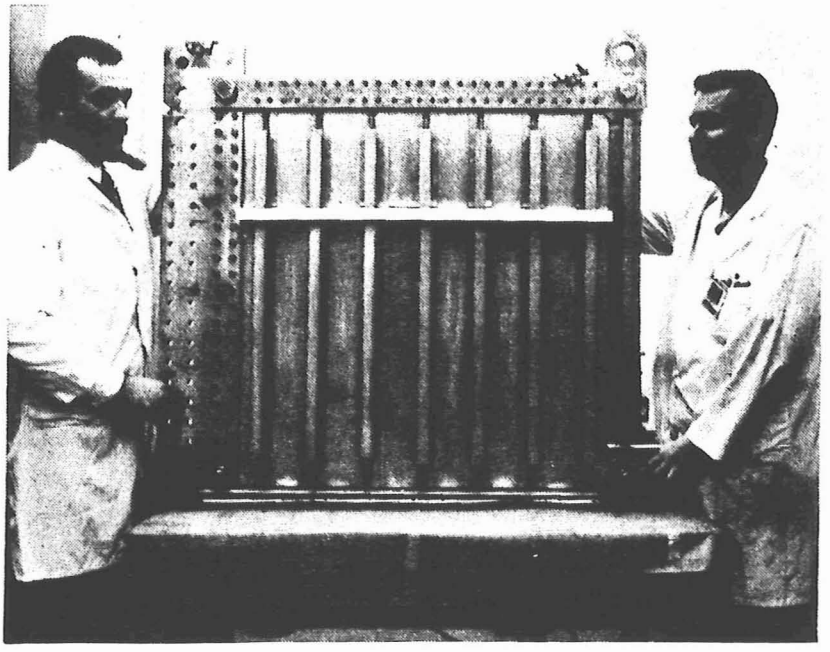

Figure 2-5. Frame Side of Completed Stiffened Panel and Test Fixture Assembly (129951B)

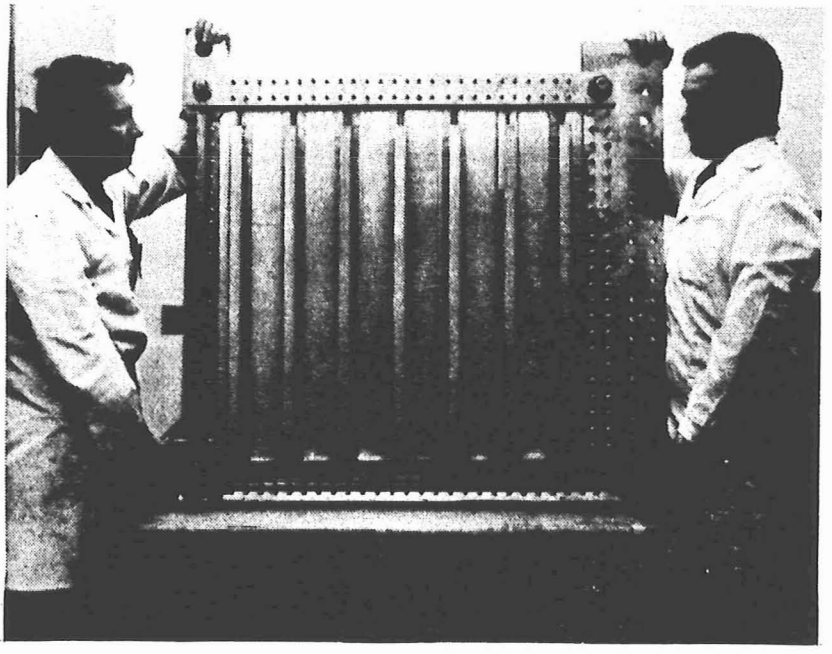

Figure 2-6. Completed Stiffened Panel and Test Fixture Assembly (129953B)

SECTION 3

TESTING OF STIFFENED PANEL

The B/Al stiffened panel was tested at NASA-MSFC in the test rig shown in Figures 3-1 and 3-2. The photograph in Figure 3-3 clearly shows the unidirectional compression cap and its fasteners for attachment to the titanium tee splice. Figure 3-4 shows the rugged cantilever support structure that reacts both the shear and normal stresses in the web as well as axial loads in the caps. Note that lateral instability was prevented by the fixture as shown in Figures 3-1 through 3-4. Design ultimate loads are achieved by the simultaneous loading of Load A = 445 kN (100,000 lb) and Load B = 890 kN (200,000 lb), as indicated in Figures 1-1 and 3-1. Strain gages shown in Figure 3-5 were installed at NASA-MSFC.

Four test loading conditions were performed. The hydraulic cylinder pressure readings were used for reference in setting the load steps with the final adjustment being made in accordance with the load cell readings. The instrumentation (strain gages),

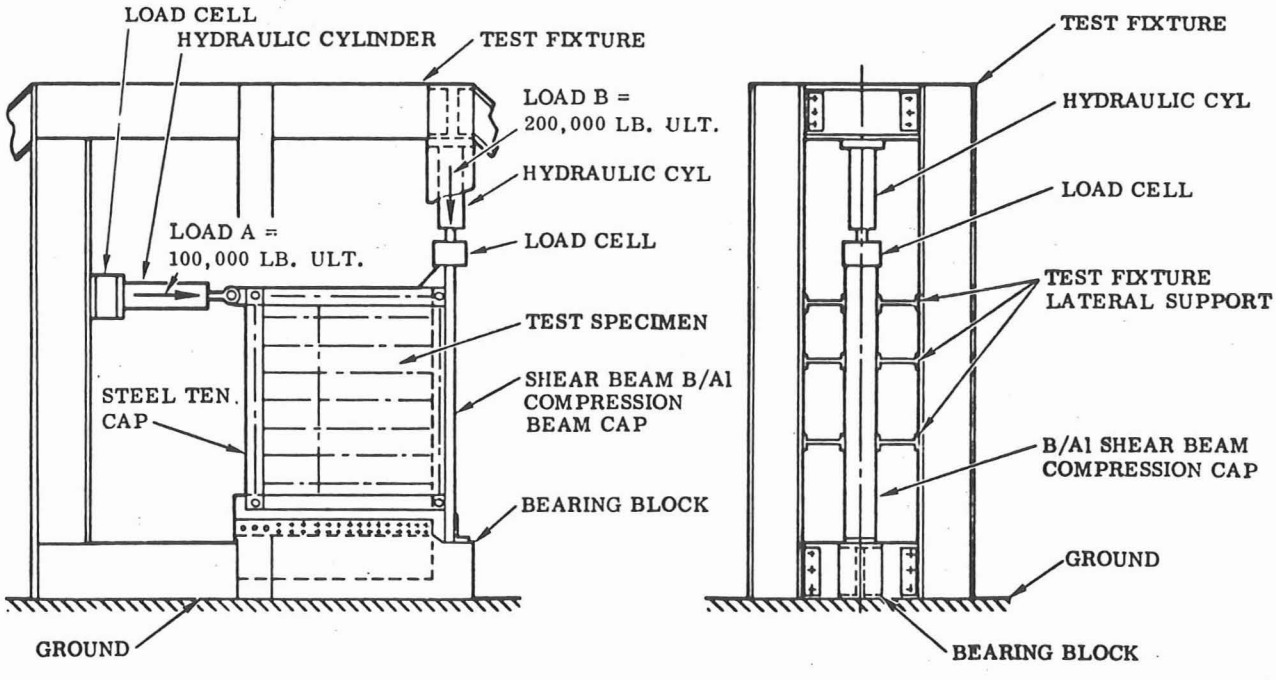

NOTE: Load A = 445 kN
Load B = 890 kN

Figure 3-1. Test Rig, B/Al Stiffened Panel

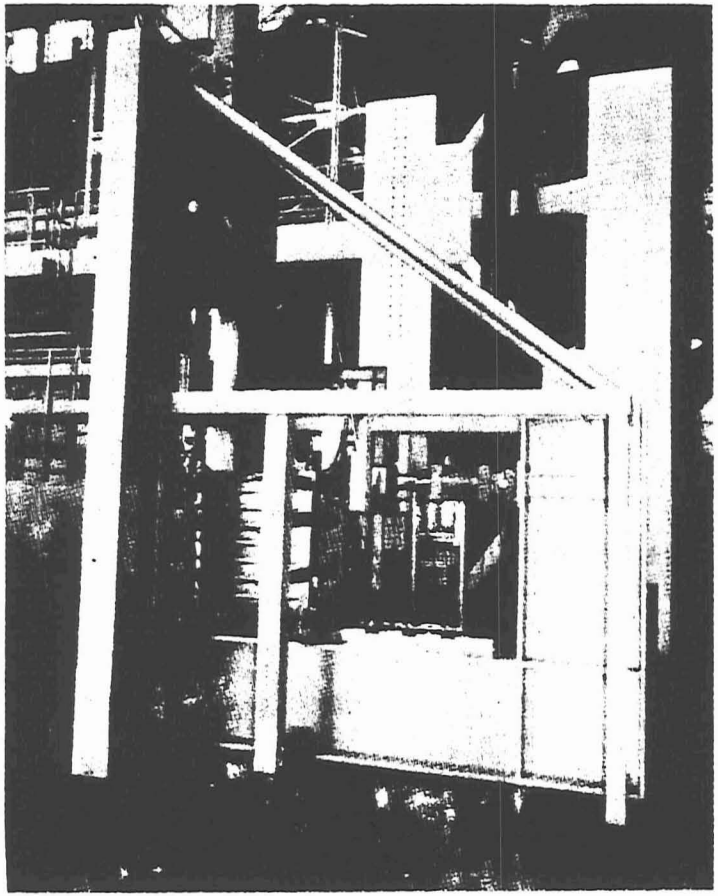

Figure 3-2. Test Rig and Setup of Stiffened Panel at NASA-MSFC (25093CVD8406)

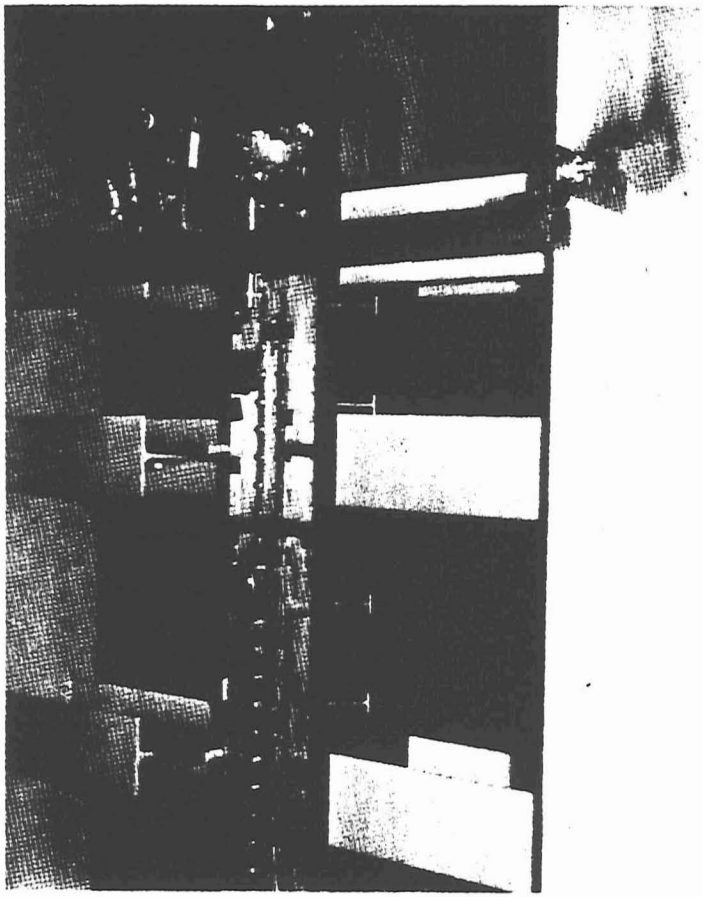

Figure 3-3. Closeup View of Test Rig Showing UD B/Al Compression Cap (25093CVD8408)

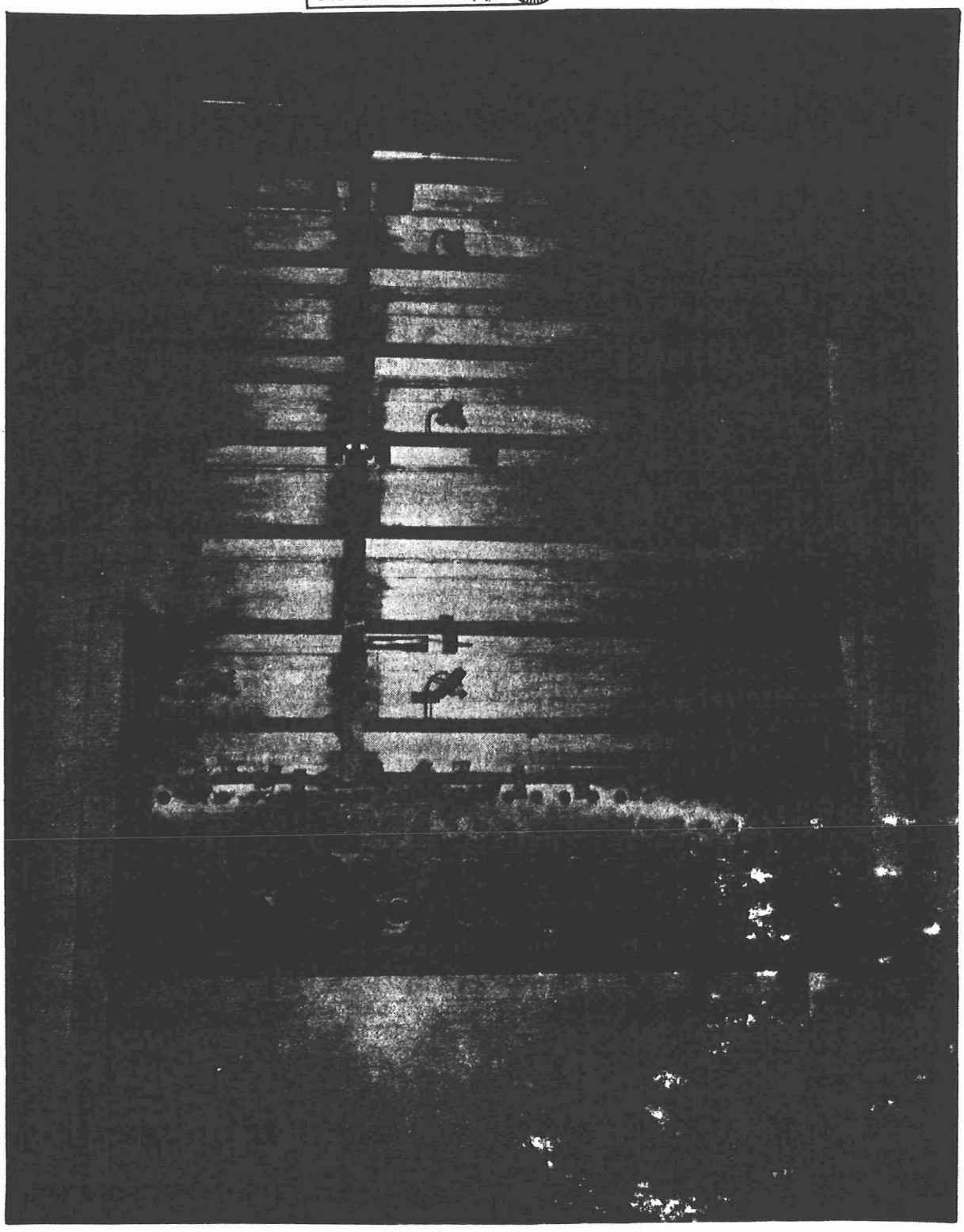

Figure 3-4. Closeup View of Test Rig Showing Rugged Cantilever Support at Lower Part of Photograph (29053CVD8412)

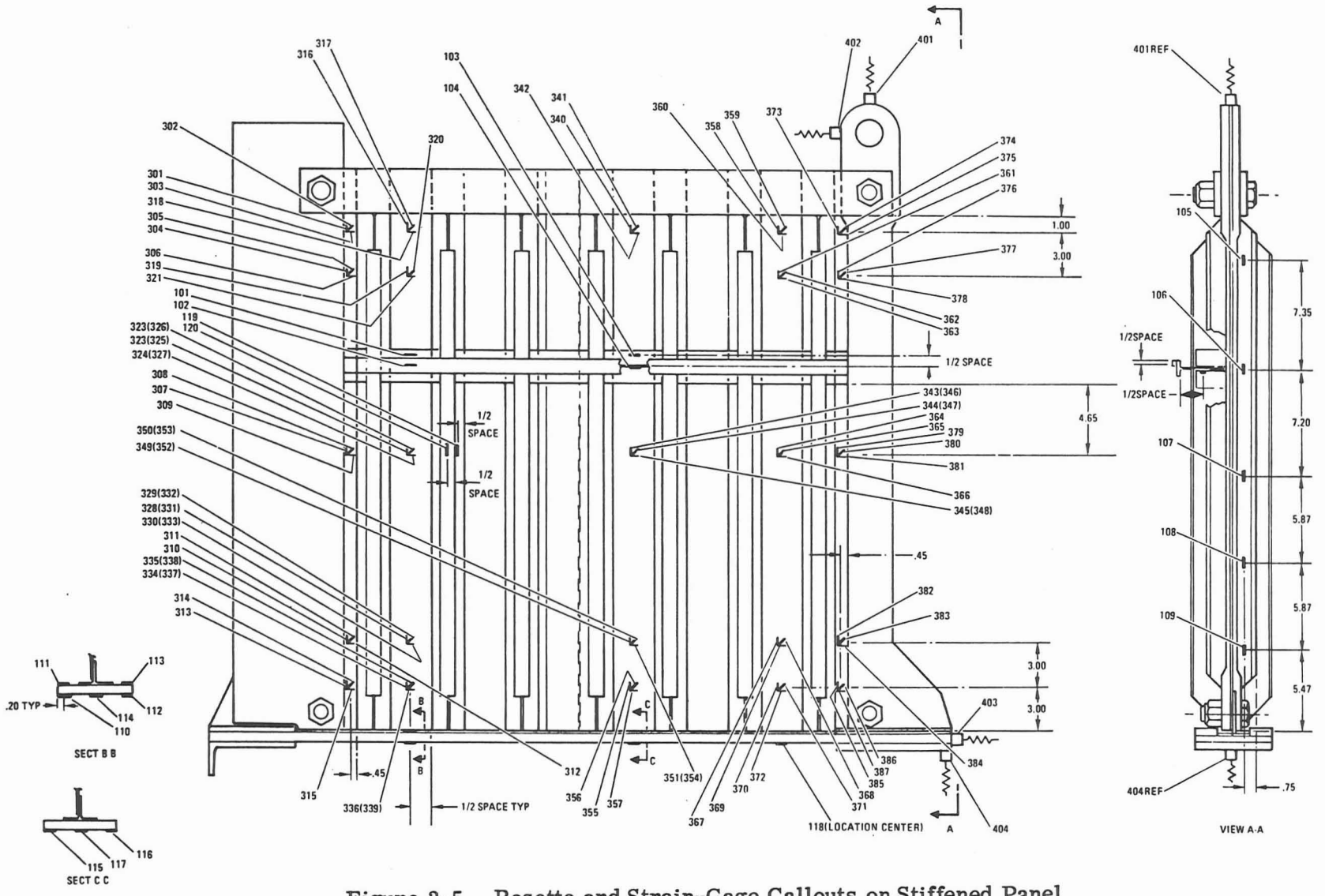

Figure 3-5. Rosette and Strain-Gage Callouts on Stiffened Panel

including the load cells, were calibrated initially and a "zero" reading taken immediately before and after each test condition. Recorded instrumentation included 20 uniaxial strain gages, 29 rosette strain gages, 4 deflection indicators, and 2 load cells, and the hydraulic cylinder pressures were monitored on pressure gages. For each test condition, data was scanned at each load increment including the initial and final zero readings. At failure, the hydraulic load maintainer was unloaded as quickly as possible. The tests were conducted remotely from the hydraulic control room. The test loading conditions were performed as follows in the order shown:

Condition 1

Load B $\equiv 2 \times$ Load A

Initial Load A = zero

Increment of Load A = 22.2 kN (5000 lb)

Maximum Load A = 335 kN (75,000 lb)

Condition 2

Load B $\equiv$ zero

Initial Load A = zero

Increment of Load A = 22.2 kN (5000 lb)

Maximum Load A = 335 kN (75,000 lb)

Condition 3

Load A $\equiv$ zero

Initial Load B = zero

Increment of Load B = 45 kN (10,000 lb)

Maximum Load B = 670 kN (150,000 lb)

Condition 4A

Load B $\equiv 2 \times$ Load A

Initial Load A = zero

Increment of Load A = 45 kN (10,000 lb)

Ultimate Load A = 445 kN (100,000 lb) (held for 6 minutes, then test resumed)

Maximum Load A = 490 kN (110,000 lb) (partial failure, automatic unloading)

Condition 4B

Load B ≡ 2 × Load A

Initial Load A = zero

Increment of Load A = 45 kN (10,000 lb)

Maximum Load A = 178 kN (40,000 lb) (complete failure)

Partial failure occurred at 110% of design ultimate load. The primary failure, sheared spotwelds in the web splice, was not apparent after Condition 4A, although a small split in a stiffener flange near the skin splice was observed. An attempt was then made to reload the panel to design ultimate load, Condition 4B. Complete failure occurred during Condition 4B for Load A = 178 kN (40,000 lb) and Load B = 356 kN (80,000 lb). Failure of the skin splice spotwelds was still not apparent to the eye, although the stiffener flange failure was visible (see Figure 3-6). This testing verified the design and manufacturing concepts used on the program and further proved that B/Al can be used with a high degree of confidence in reusable space vehicles such as the Space Shuttle.

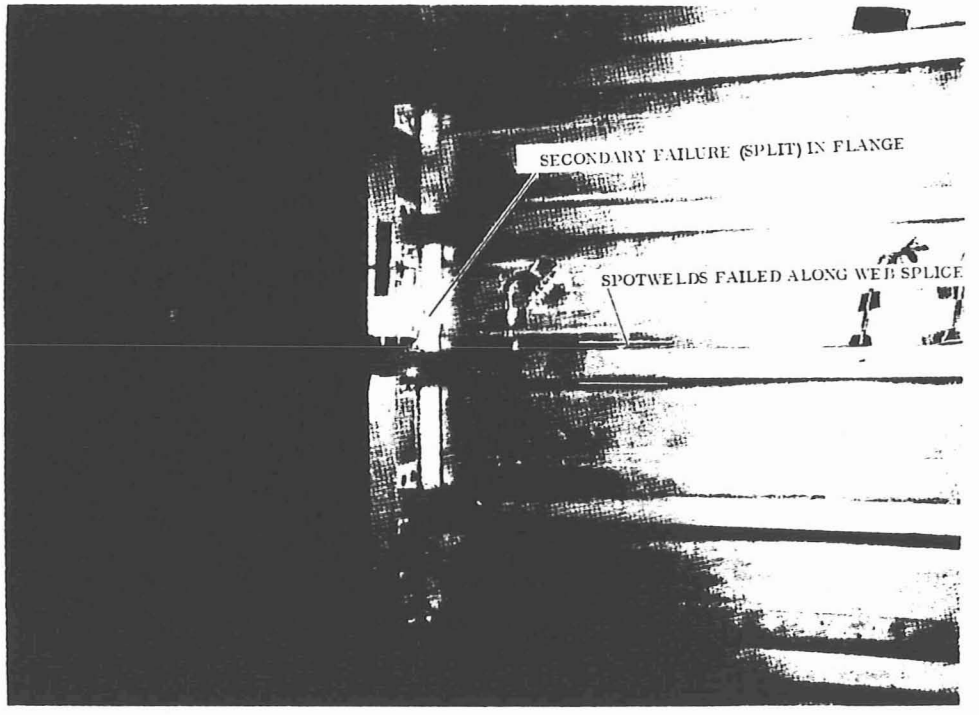

Figure 3-6. Visible Failure at Stiffener Attachment; Spotweld Failures not Apparent (25093CVD8407)

SECTION 4

BORON/ALUMINUM MATERIAL PROPERTIES

The material properties discussed in this section were obtained from data generated earlier in the program (Reference 2). For clarity, the remainder of the tabulations, figures, and sample calculations in this report are in English units only.

4.1 BASIC MATERIAL PROPERTIES

The stiffened panel compression cap and stiffeners were fabricated from as-received (Condition F) diffusion-bonded, unidirectional B/Al, while the web was made from diffusion-bonded ±45-degree heat-treated B/Al. The design mechanical properties that were established for these materials are:

UD, Condition F, Boron/Aluminum (6061 Alloy)

F_{tu_x} *	= 1276 MPa (185 ksi)	E_{t_x}	= 224 GPa (32.5 msi)
F_{tu_y}	= 133 MPa (19.3 ksi)	E_{t_y}	= 121 GPa (17.5 msi)
ϵ_{u_x}	= 0.0061 m/m	$F_{su_{xy}}$	= 55 MPa (8 ksi)
ϵ_{u_y}	= 0.0020 m/m	G_{xy}	= 41 GPa (6 msi)
ν_{xy}	= 0.23	* x refers to the zero-degree direction of the laminate	

±45-Degree STA Boron/Aluminum (6061 Alloy)

F_{tu_x} *	= F_{ty_y} = 248 MPa (36 ksi)	$F_{su_{xy}}$	= >390 MPa (56 ksi)
ϵ_{u_x}	= ϵ_{u_y} = 0.010 m/m	G_{xy}	= 806 Pa (11.6 msi)
E_{t_x}	= E_{t_y} = 172 GPa (25 msi)	ν_{xy}	= ν_{yx} = 0.31

Tensile and shear stress-strain curves for ±45-degree heat-treated B/Al are shown in Figures 4-1 and 4-2 respectively. A plot of the plasticity factor for tension ($\eta = E_{sec}/E$) is shown in Figure 4-3. By using test data, plots of Poisson's ratio versus stress and the plasticity factor are shown in Figures 4-4 and 4-5 respectively.

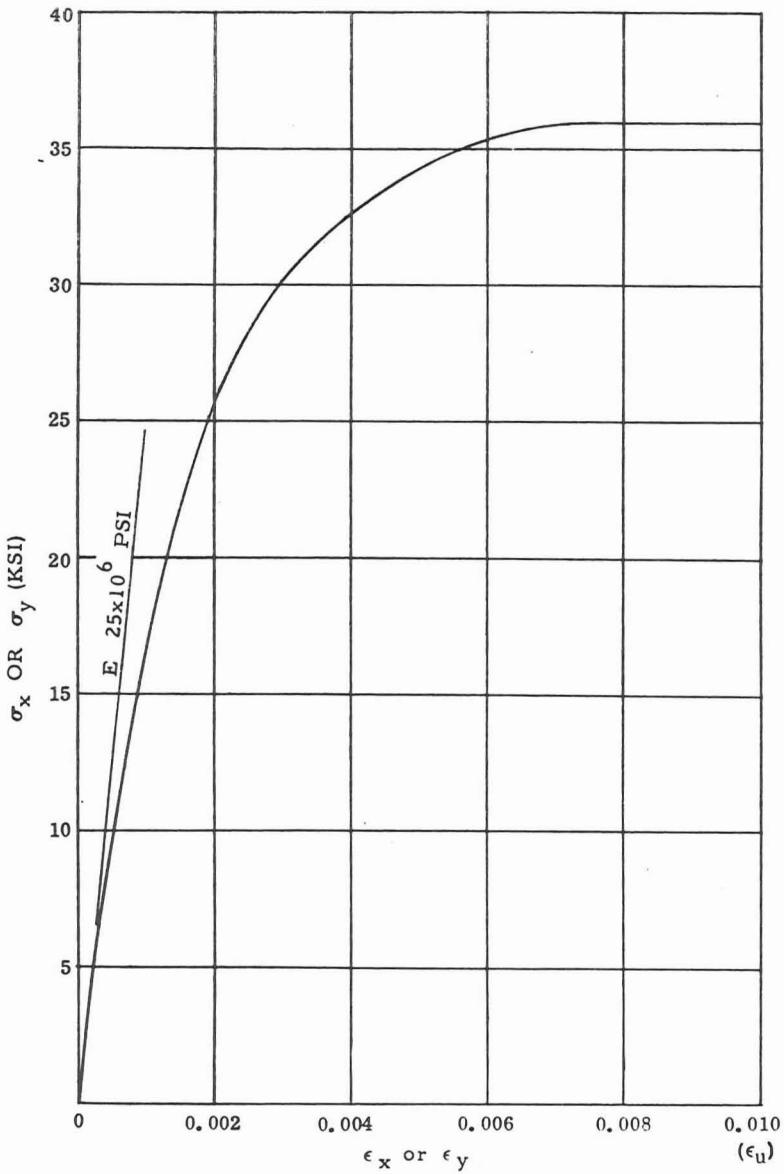

Figure 4-1. Stress/Strain Curve of ±45-degree, STA, B/Al

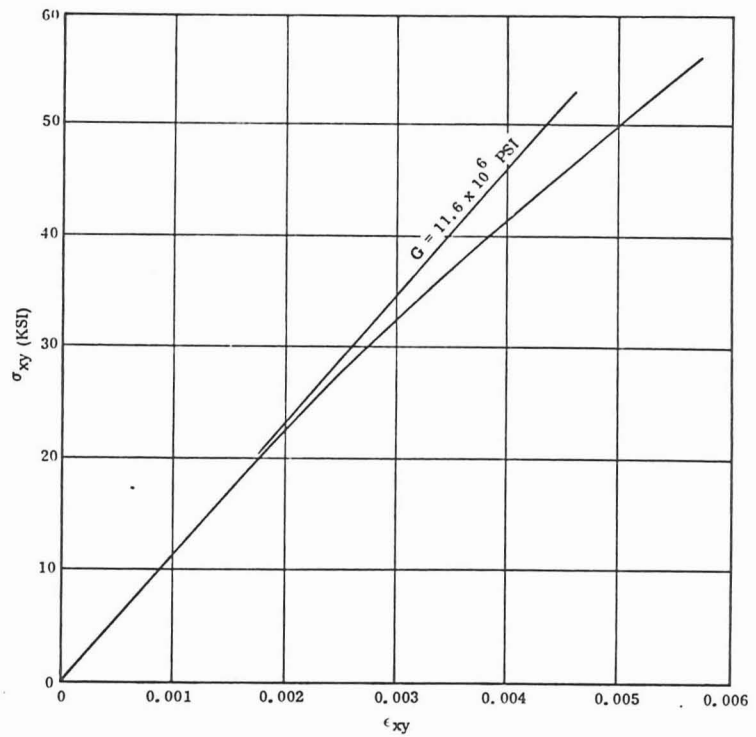

Figure 4-2. Shear Stress/Strain Curve of ±45-degree, STA, B/Al

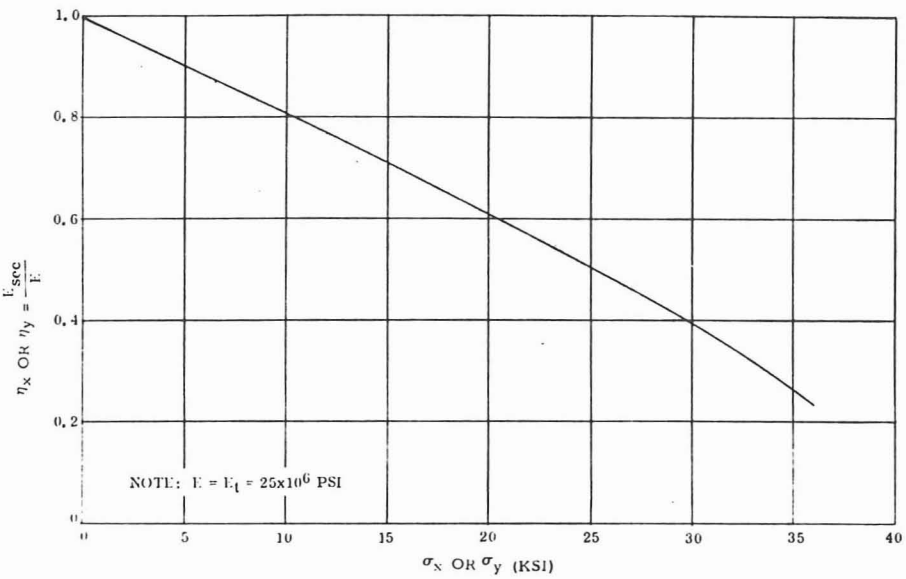

Figure 4-3. Plasticity Factor $\eta = E_{sec}/E$ for ±45-degree, STA, B/Al

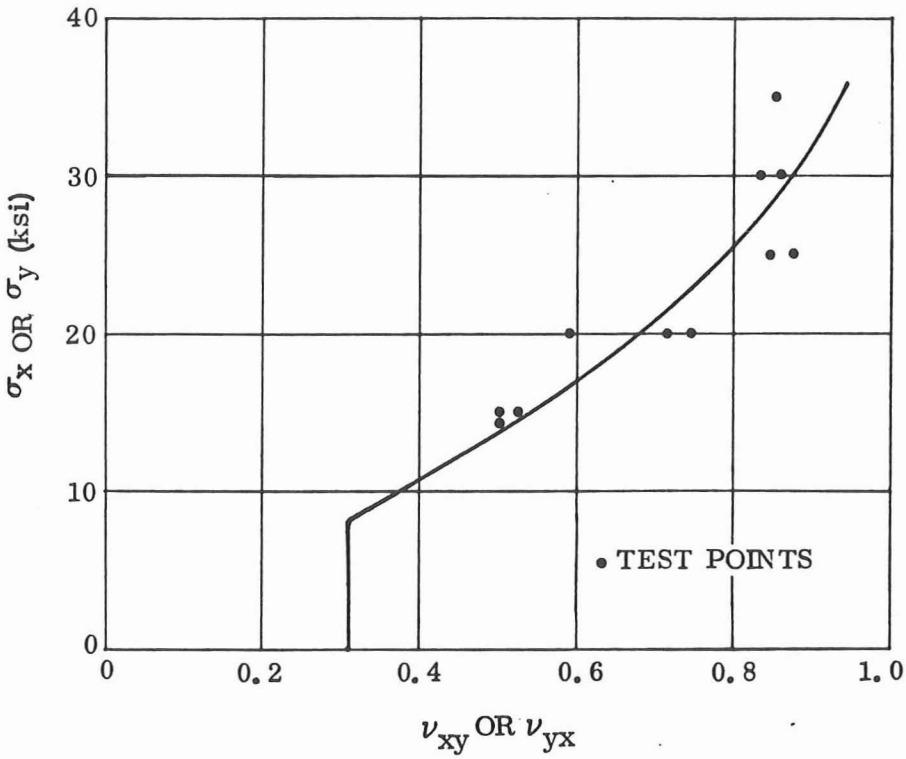

Figure 4-4. Poisson's Ratio for ±45-degree, STA, B/Al

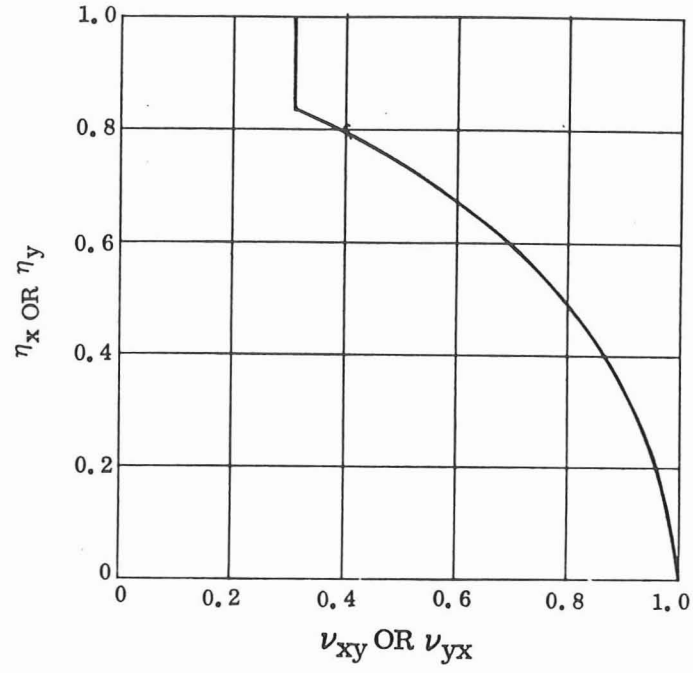

Figure 4-5. Poisson's Ratio Versus Plasticity Factor for ±45-degree, STA, B/Al

Compressive mechanical properties for the web material were assumed to be the same as that for tension because of the lack of adequate compressive test data.

4.2 INELASTIC STIFFNESS OF ±45 DEGREE HEAT-TREATED BORON/ALUMINUM

Since the stress-strain and stress-Poisson's ratio responses for ±45-degree heat-treated B/Al are quite nonlinear as shown in Figures 4-1 through 4-5, some inelastic theory had to be established for the orthotropic web in the finite element analysis. Accordingly, it was expedient to modify the conventional orthotropic plane stress elastic stiffness coefficients (A_{ij}, D_{ij}) in the following inelastic form:

$$\left[A^I\right] = \begin{bmatrix} A^I_{xx} & A^I_{xy} & 0 \\ A^I_{xy} & A^I_{yy} & 0 \\ 0 & 0 & A^I_{66} \end{bmatrix} \qquad (4\text{-}1)$$

$$\left[D^I\right] = \begin{bmatrix} D^I_{xx} & D^I_{xy} & 0 \\ D^I_{xy} & D^I_{yy} & 0 \\ 0 & 0 & D^I_{66} \end{bmatrix} \tag{4-2}$$

where

$$A^I_{xx} = \frac{\eta_x E_x t}{(1-\nu_{xy}\nu_{yx})}, \quad A^I_{yy} = \frac{\eta_y E_y t}{(1-\nu_{xy}\nu_{yx})}$$

$$A^I_{xy} = \sqrt{\nu_{yx} A^I_{xx} \nu_{xy} A^I_{yy}}, \quad A^I_{66} = \eta_s G_{xy} t \tag{4-3}$$

and

$$D^I_{xx} = \frac{\eta_x E_x t^3}{12(1-\nu_{xy}\nu_{yx})}, \quad D^I_{yy} = \frac{\eta_y E_y t^3}{12(1-\nu_{xy}\nu_{yx})}$$

$$D^I_{xy} = \sqrt{\nu_{yx} D^I_{xx} \nu_{xy} D^I_{yy}}, \quad D^I_{66} = \frac{\eta_s G_{xy} t^3}{12} \tag{4-4}$$

The terms A^I_{ij} are the extensional stiffness coefficients, and D^I_{ij} are the flexural stiffness coefficients. Actually, only the values of A^I_{ij} are input to the plane inelastic finite element analysis for this work.

In lieu of biaxial test data, it was decided that inelastic material properties from uniaxial tests would suffice for determining the inelastic stiffness coefficients for a biaxial stress state. Maxwell's reciprocal theorem

$$(\nu_{yx} E_x = \nu_{xy} E_y)$$

has been discarded in this report and Poissons' ratios are found independently for each individual stress. The possibility of obtaining theoretical biaxial material properties by use of lamination theory was not considered at this time, but it does offer an interesting alternative provided sufficient unidirectional test data becomes available.

The inelastic stiffness coefficients have been plotted in Figures 4-6 through 4-9 by the use of Figure 4-5 and Equation 4-3, where the elastic modulus was assumed to be 172 Pa (25 msi). Tension and compression properties were assumed to be identical. Inelastic shear stresses did not occur in the finite-element analysis; thus, the curve for A^I_{66}/t was not needed.

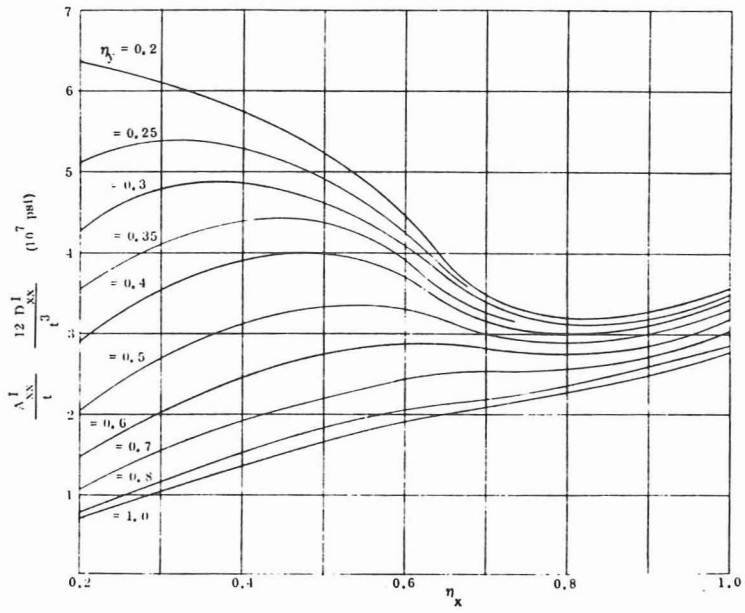

Figure 4-6. Inelastic Stiffness Coefficients for ±45-degree, STA, B/Al

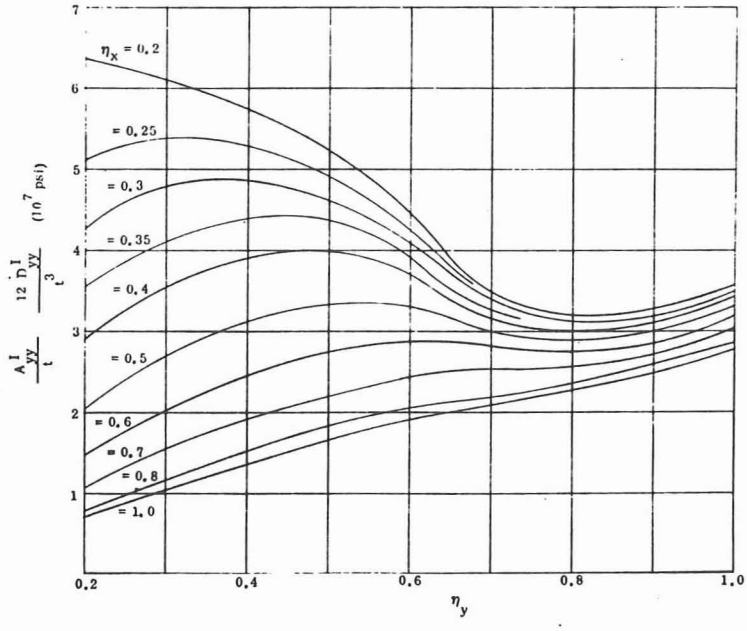

Figure 4-7. Inelastic Stiffness Coefficients for ± 45-degree, STA, B/Al

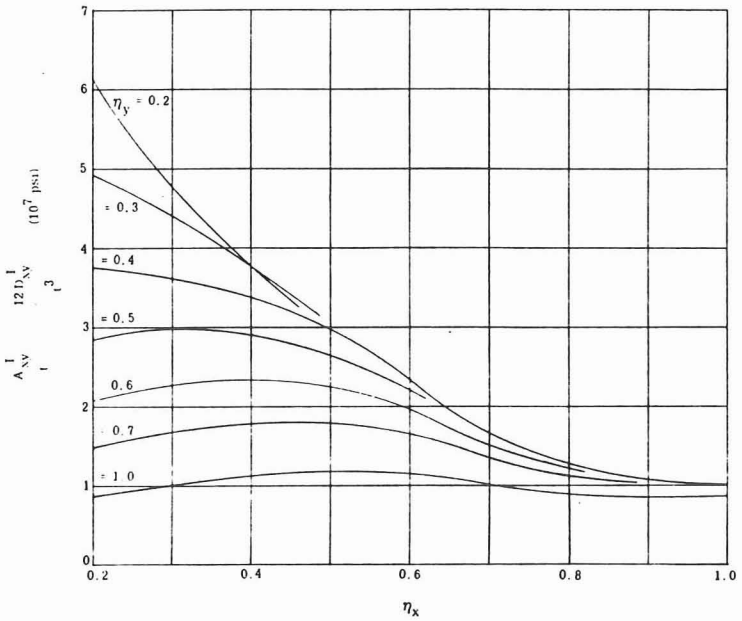

Figure 4-8. Inelastic Stiffness Coefficients for ±45-degree, STA, B/Al

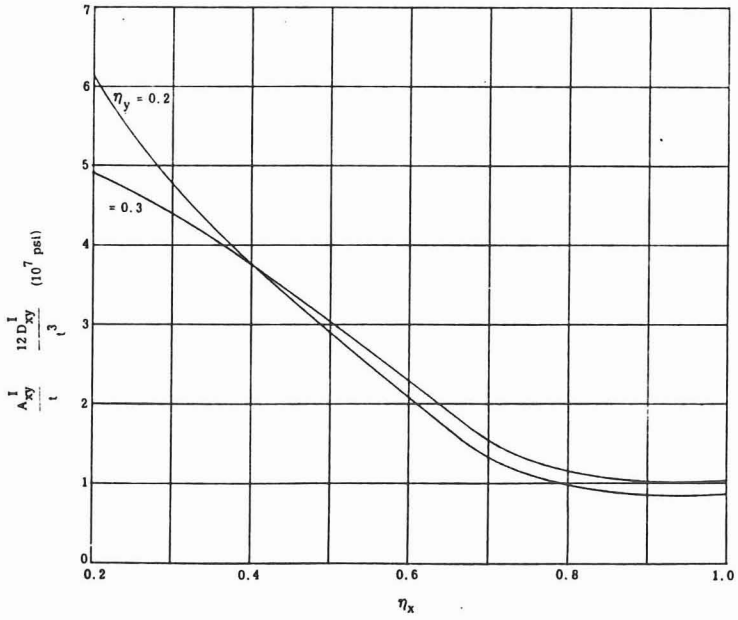

Figure 4-9. Inelastic Stiffness Coefficients for ±45-degree, STA, B/Al

An example of locating a point for plotting the curves found in Figures 4-6 through 4-9 is presented below for a point ($\eta_x = 0.5$, $\eta_y = 0.6$) in Figure 4-6.

Step 1

For $\eta_x = 0.5$ and $\eta_y = 0.6$, find that $\nu_{xy} = 0.79$ and $\nu_{yx} = 0.69$, respectively from Figure 4-5.

Step 2

Compute A^I_{xx}/t by Equation 4-3:

$$A^I_{xx}/t = \frac{\eta_x E_x}{1-\nu_{xy}\nu_{yx}}$$

$$= \frac{0.5 \times 25 \times 10^6}{1-0.79 \times 0.69}$$

$$= 2.75 \times 10^7 \text{ psi}$$

which agrees with Figure 4-6.

Since the web must be stable at ultimate load, it was necessary to determine the inelastic buckling allowables for ±45-degree heat-treated B/Al plates. It was found expedient to arbitrarily assume that the compressive plastic buckling factors developed by Stowell (Reference 7) for isotropic metals would be approximately valid for ±45-degree heat-treated B/Al. Stowell's factors are shown in Table 4-1, and corresponding inelastic buckling correction curves for ±45-degree heat-treated B/Al, are presented in Figures 4-10 and 4-11. The shear plasticity factor η_s was also included in Table 4-1 and Figure 4-10 for possible use in shear buckling analysis. The calculated elastic buckling stress (σ_{cr}/η or τ_{cr}/η_s)is located on the abscissa. Then, the inelastic buckling stress (σ_{cr} or τ_{cr}) is read on the ordinate in accordance with the appropriate curve.

Table 4-1. Plasticity Factors (η) for Compressive and Shear Buckling

Structure	η	Curve
Long flange, one unloaded edge simply supported and the other free	$\frac{E_{sec}}{E}$	A
Long flange, one unloaded edge clamped and the other free	$\frac{E_{sec}}{E}\left(0.428 + 0.572\sqrt{\frac{1}{4} + \frac{3}{4}\frac{E_{tan}}{E_{sec}}}\right)$	B
Long plates, both unloaded edges simply supported	$\frac{E_{sec}}{E}\left(\frac{1}{2} + \frac{1}{2}\sqrt{\frac{1}{4} + \frac{3}{4}\frac{E_{tan}}{E_{sec}}}\right)$	C
Long plate, both unloaded edges clamped	$\frac{E_{sec}}{E}\left(0.352 + 0.648\sqrt{\frac{1}{4} + \frac{3}{4}\frac{E_{tan}}{E_{sec}}}\right)$	D
Short plate loaded as a column $\left(\frac{L}{b} \ll 1\right)$	$\frac{1}{4}\frac{E_{sec}}{E} + \frac{3}{4}\frac{E_{tan}}{E}$	E
Square plate loaded as a column $\left(\frac{L}{b} = 1\right)$	$0.114\frac{E_{sec}}{E} + 0.886\frac{E_{tan}}{E}$	F
Long column $\left(\frac{L}{b} \gg 1\right)$	$\frac{E_{tan}}{E}$	G
Plate in shear	$\frac{G_{sec}}{G}$	H

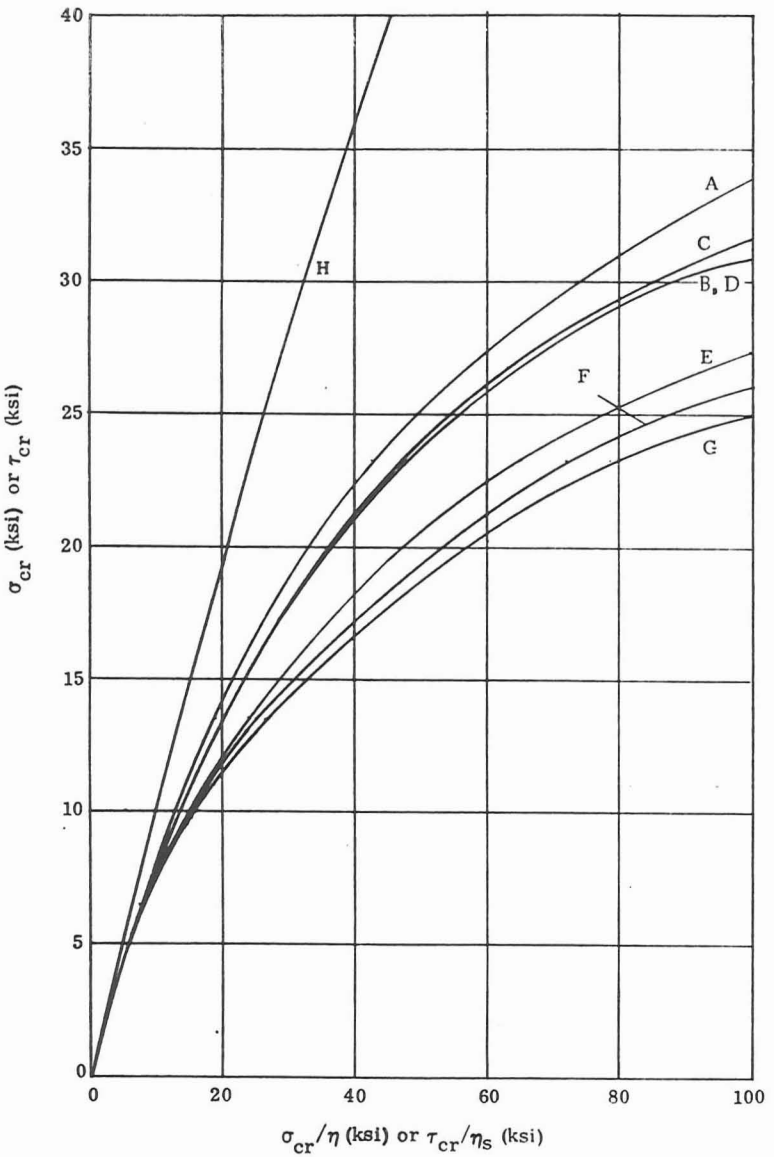

Figure 4-10. Flat-Plate Plastic Buckling Correction Curves for ±45-degree, STA, B/Al

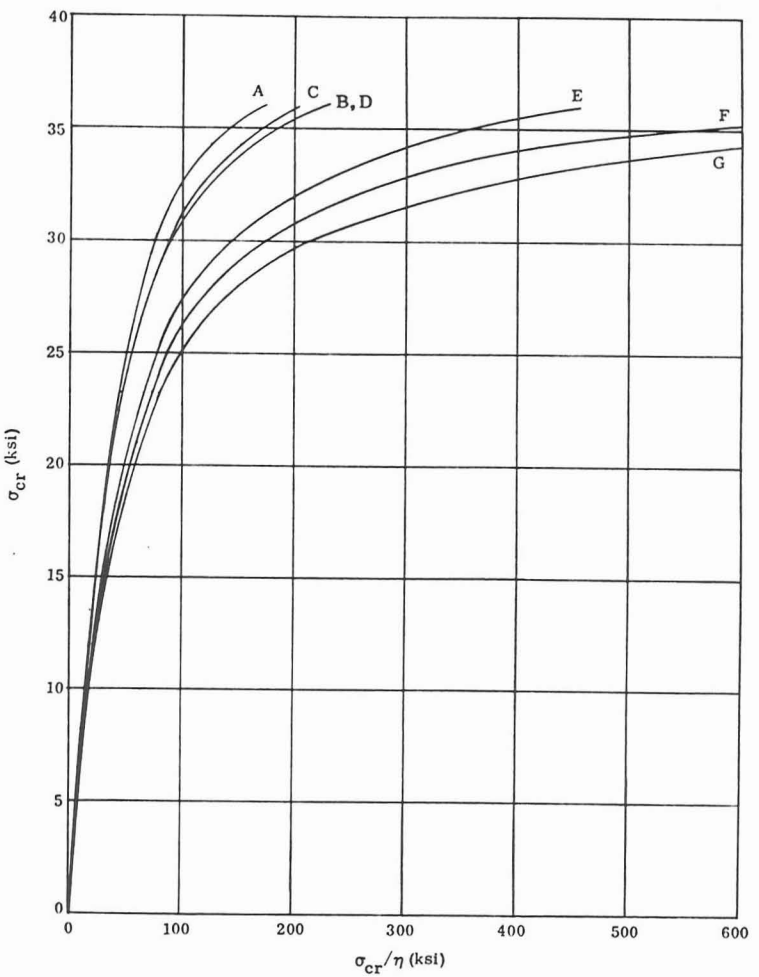

Figure 4-11. Flat-Plate Plastic Buckling Correction Curves for ±45-degree, STA, B/Al

SECTION 5

FINITE ELEMENT ANALYSIS

A plane stress orthotropic finite element analysis was performed on the CDC 6400 computer for the model shown in Figure 5-1. All stiffeners and caps were considered to carry axial loads only. All elastic solutions were obtained by assuming the elastic modulus of the web to be 138 GPa (20 msi) rather than 172 GPa (25 msi) because the lower value appeared to be more realistic for modest stress levels. An elastic analysis was obtained for Load Conditions 2, 3, and 4A, where Condition 4A coincides with Condition 1. Load Condition 1 was terminated at 75% of ultimate load. Since load Conditions 3 and 4A involved substantial inelastic stresses in the ±45-degree heat-treated B/Al web, iterative inelastic finite element solutions were obtained by use of the technique proposed in this report. An example of the technique employed for the determination of the inelastic stiffness coefficients A_{ij}^I/t^* for use in the iterative inelastic finite element analysis is: Assume that after iteration Number 3 the calculated biaxial stresses in an element of the web are

$$\sigma_x = -25,000 \text{ psi} \qquad \sigma_y = -17,000 \text{ psi}$$

$$\sigma_{xy} = -8,000 \text{ psi}$$

Now determine the appropriate inelastic stiffness coefficients A_{ij}^I/t for use in iteration number 4.

Step 1†

From Figure 4-3, $\eta_x = 0.5$ for $\sigma_x = 25,000$ psi and $\eta_y = 0.67$ for $\sigma_y = 17,000$ psi

Step 2

From Figure 4-6, for $\eta_x = 0.5$ and $\eta_y = 0.67$

$A_{xx}^I = 2.4 \times 10^7$ psi

Step 3

From Figure 4-7, for $\eta_x = 0.5$ and $\eta_y = 0.67$

$A_{yy}^I/t = 3.08 \times 10^7$ psi

---

* As noted the values for A_{ij}^I/t rather than A_{ij}^I are input to the computer program.

† It was stated earlier that tension and compression mechanical properties of the ±45-degree material were assumed identical.

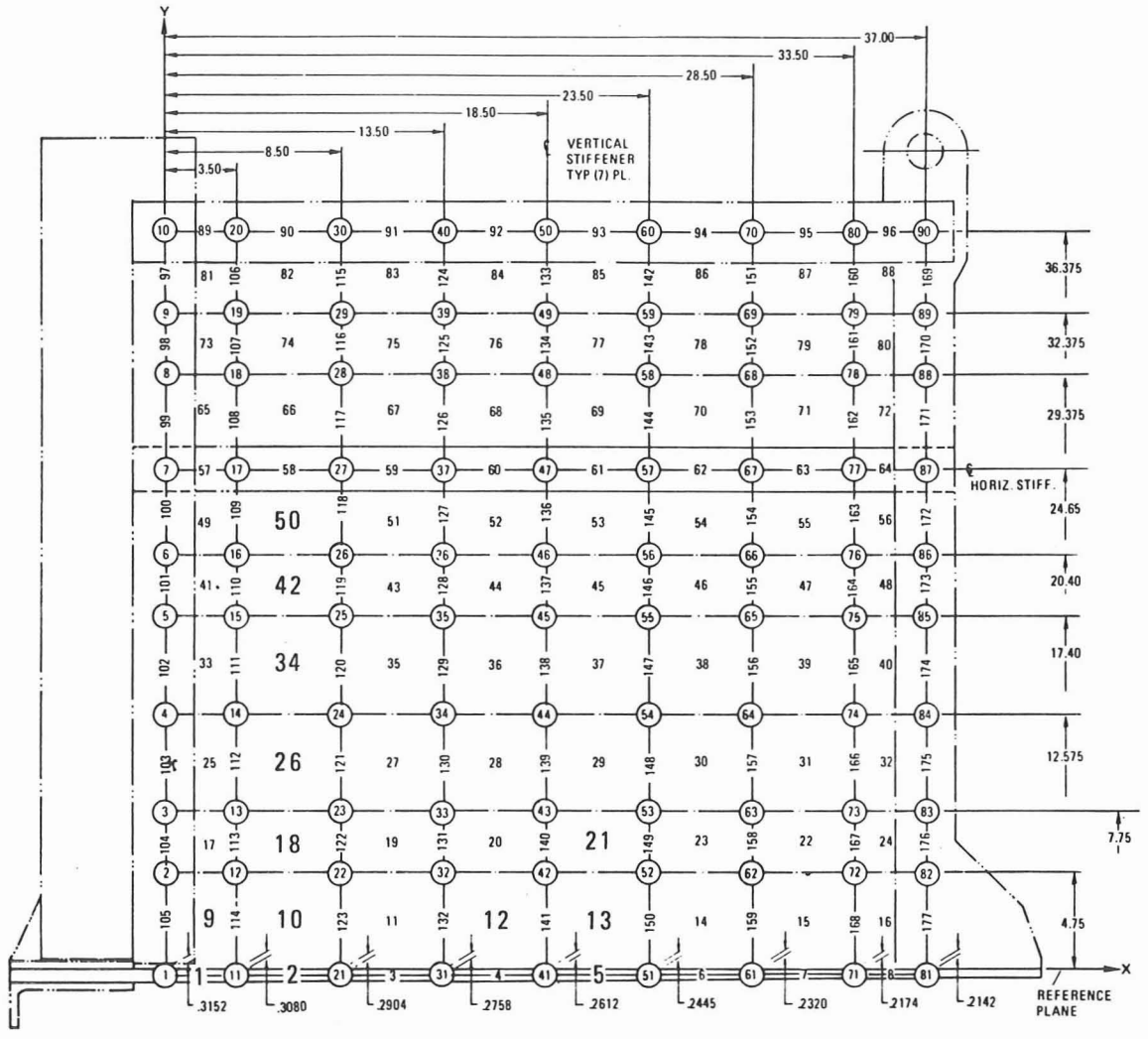

Figure 5-1. Finite Element Model

Step 4

From Figure 4-8, for $\eta_x = 0.5$ and $\eta_y = 0.67$

$A^I_{xy}/t = 2.0 \times 10^7$ psi

Step 5

Since the shear stress is elastic ($\eta_s = 1.0$) as shown by Figure 4-2 or 4-10 (curve H) for $\sigma_{xy} = -8{,}000$ psi, the shear modulus ($G_{xy} = 11.6 \times 10^6$ psi) is used.

The value for A^I_{66}/t by Equation 4-3 is

$A^I_{66}/t = G_{xy} = 80$ GPa (11.6 msi)

When the calculations for A_{ij}^{I}/t are the same as those for the previous finite element iteration, that particular element is considered to have converged. When convergence has been reached for all elements of the web, the solution is complete.

The inelastic analysis involved the iterative employment of the inelastic stiffness coefficients A_{ij}^{I} of the web found in Figures 4-6 through 4-9. Since the shear stress was elastic during all of the load conditions, it was unnecessary to consider the use of the inelastic shear modulus $\eta_s G_{xy}$, which could be obtained from Figure 4-2. However, the calculated elastic shear buckling allowable $\sigma_{xy_{cr}}/\eta_s$ (or τ_{cr}/η_s) of any panel must be corrected for plasticity by use of curve H in Figure 4-10. Also, theoretical compressive elastic buckling calculations σ/η need to be corrected for plasticity by the appropriate curve in Figures 4-10 or 4-11 according to the definitions found in Table 4-1.

The inelastic solutions on the computer required nine and five iterations for Load Conditions 4A and 3, respectively. The maximum web stresses occurred in Element 9, and the maximum stresses in the compression cap occurred in Element 1. Accordingly, the stresses in these elements from both the elastic and inelastic solutions are shown for Conditions 2, 3, and 4A in Table 5-1. Note that the maximum discrepancy between the elastic and inelastic analyses involves the stress σ_y, which is perpendicular to the compression cap.

Table 5-1. Stresses in Elements 1 and 9 for Elastic and Inelastic Finite Element Solutions

LOAD CONDITION (LB.)	ELEMENT	STRESS COMPONENT	STRESS (psi)	
			ELASTIC ANALYSIS	INELASTIC ANALYSIS
2	1	σ_x	-17,190	
A = 75,000	9	σ_x	- 9,300	
		σ_y	- 2,400	
		σ_{xy}	-10,000	
3	1	σ_x	-30,951	-30,960
B = 150,000	9	σ_x	-18,670	-19,290
		σ_y	- 4,700	- 7,340
		σ_{xy}	- 1,590	- 2,160
4A	1	σ_x	-64,180	-66,360
A = 100,000	9	σ_x	-37,300	-33,600
+		σ_y	- 9,470	-25,590
B = 200,000		σ_{xy}	-15,550	-20,340

SECTION 6

CORRELATION OF STRAIN GAGE DATA WITH ANALYSIS

Correlation between strain gage readings with the results of the inelastic finite element analysis are shown for a highly stressed region in Figure 6-1, which includes two web elements and an element of the compression cap. Note that for the strain ϵ_x, excellent agreement is obtained in the compression cap and good agreement is found in the web. Good agreement is obtained in the web for the shearing strain ϵ_{xy}, while fair agreement is found in the web for the strain ϵ_y.

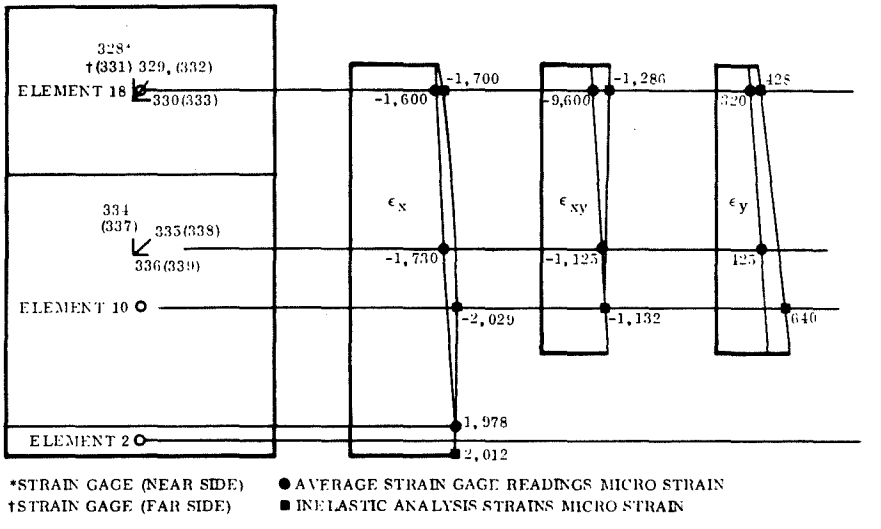

Figure 6-1. Strains in Elements 2 (Compression Cap), 10 (Web), and 18 (Web) for Load Condition 4A (Design Ultimate Load)

Since strain gages in Elements 2 and 18 are concentric with the element geometries, detailed strain correlation plots for both elastic and inelastic finite element solutions are shown in Figures 6-2 and 6-3, respectively. Elastic analysis strains are plotted along with the strain gage readings, while the inelastic strains are obtained only by the iterative analysis at ultimate load. Also, average strain gage readings are compared with calculated elastic and inelastic analysis strains for the web in Table 6-1. Comparisons between calculated elastic and inelastic stresses are also shown in Table 6-1. Note that the elastic analysis resulted in a significant error for the value of ϵ_y, thus accounting for the large difference in the stress σ_y. Consequently, the elastic finite element analysis was not conservative in the y-direction.

After loading the panel to 75% of design ultimate load in Load Condition 1, the theory broke down for Load Condition 2 where only 75% of design ultimate Load A was applied. The results for Load Condition 2, shown in Figures 6-4 and 6-5, are far less accurate than those for Condition 4A. The web elastic behavior during Condition 2 could possibly

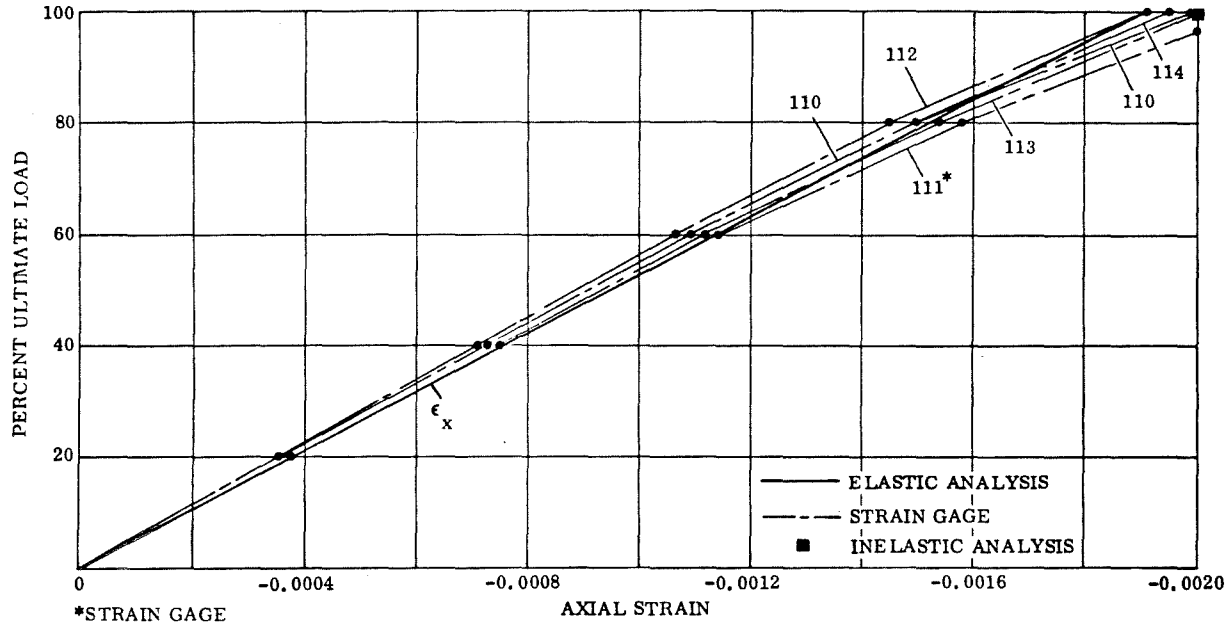

Figure 6-2. Strain Gage Readings and Theoretical Strains at Element 2 of Compression Cap for Load Condition 4A (Design Ultimate Load)

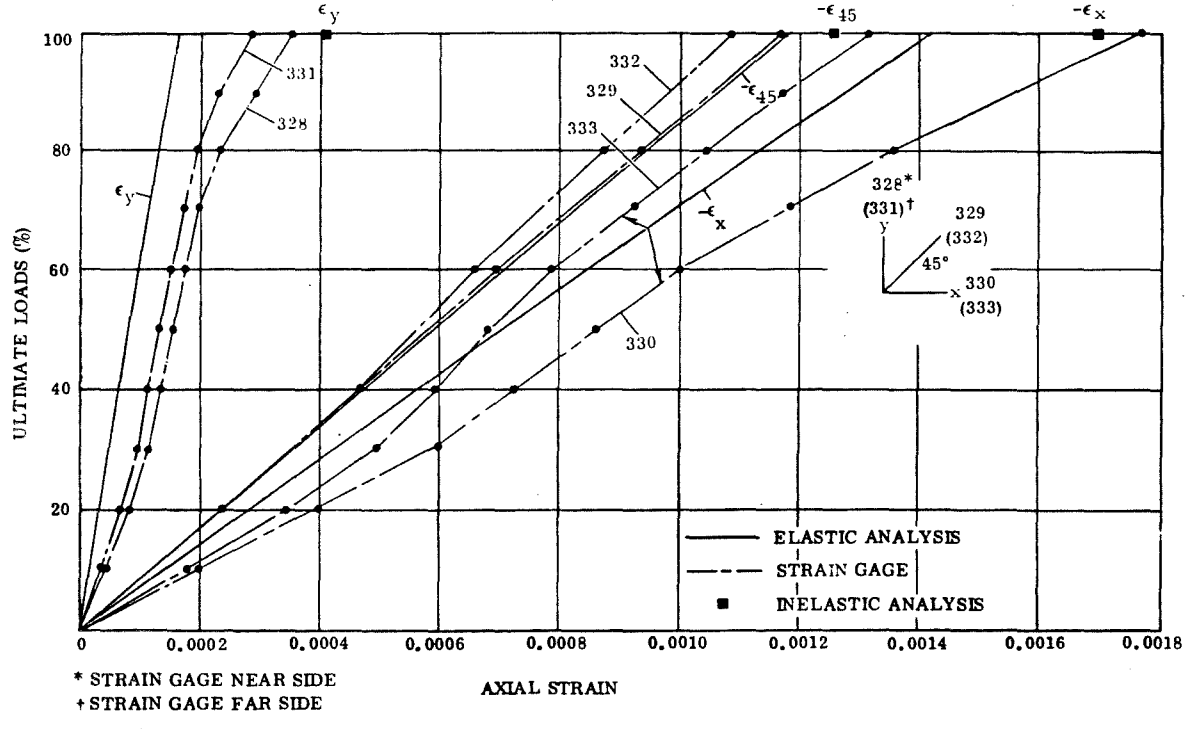

Figure 6-3. Strain Gage Readings and Theoretical Strains at Element 18 of Web for Load Condition 4A (Design Ultimate Load)

Table 6-1. Strain Gage/Rosette Analysis versus Elastic/Inelastic Analysis at Element 18 of Web for Load Condition 4A (Design Ultimate Load)

STRAIN QUANTITY	STRAIN GAGE (AVE. STRAIN)	ELASTIC ANALYSIS		INELASTIC ANALYSIS	
		STRAIN	DIFFERENCE[2] %	STRAIN	DIFFERENCE[2] %
ϵ_x	-0.000160	-0.00142	11.2	-0.001700	6.2
ϵ_y	0.000320	0.00014	56.2	0.000428	33.8
$\epsilon_{45°}$[1]	-0.001120	-0.00118	5.4	-0.001279	14.2
ϵ_{xy}[1]	-0.000960	-0.00111	15.6	-0.001286	33.9
STRESS QUANTITY		STRESS (psi)		STRESS (psi)	
σ_x		-30,400		-27,170	
σ_y		- 6,500		-17,360	
σ_{xy}		-12,900		-14,920	

(1) $\epsilon_{45°} = (1/2)(\epsilon_{xy} + \epsilon_x + \epsilon_y)$

(2) STRAIN DIFFERENCE BETWEEN ANALYSIS AND STRAIN GAGE, ASSUMING STRAIN GAGE VALUE IS CORRECT

be due to some working and/or Bauschinger effect (see Reference 8) of the matrix material during the previous inelastic loading, which could change the elastic response of the laminate. However, when the panel was later retested with Load Condition 4A, which was the same loading as Condition 1, there was remarkable repetition of the strain curves up to the limit of Load Condition 1.

The third load condition involved the application of 75% of design ultimate Load B. The results are shown in Figures 6-6 and 6-7 and in Table 6-2. Agreement between test and theory for Load Condition 3 was far better than that for Load Condition 2. It is interesting to note that Load Condition 3 resulted in inelastic stresses in the web, while Load Condition 2 was entirely elastic. Thus, it appears that, since the web had been initially stressed in the plastic range, the theory now only holds for load conditions that result in inelastic stresses. Probably, if Load Condition 2 has been performed first, much better correlation between theory and test would have been obtained for this elastic case.

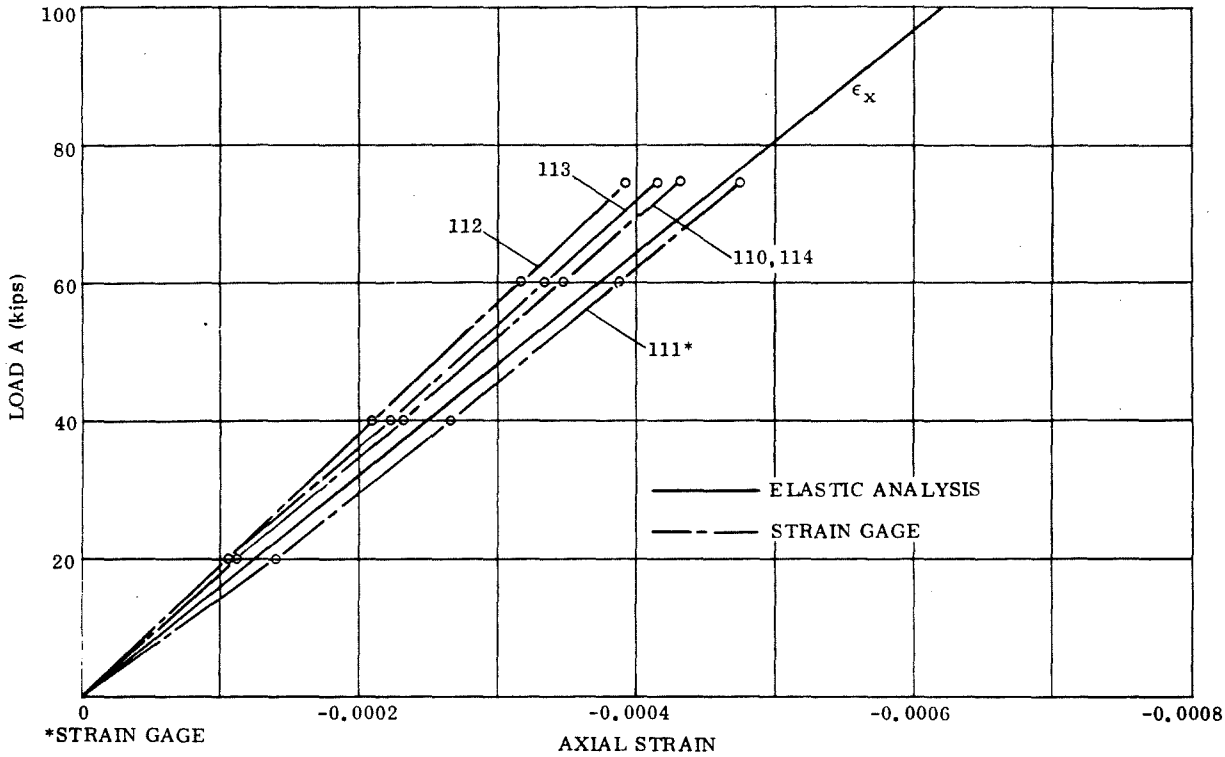

Figure 6-4. Strain Gage Readings and Theoretical Strains at Element 2 of Compression Cap for Load Condition 2 (75% of Design Ultimate Load A where Load B is absent)

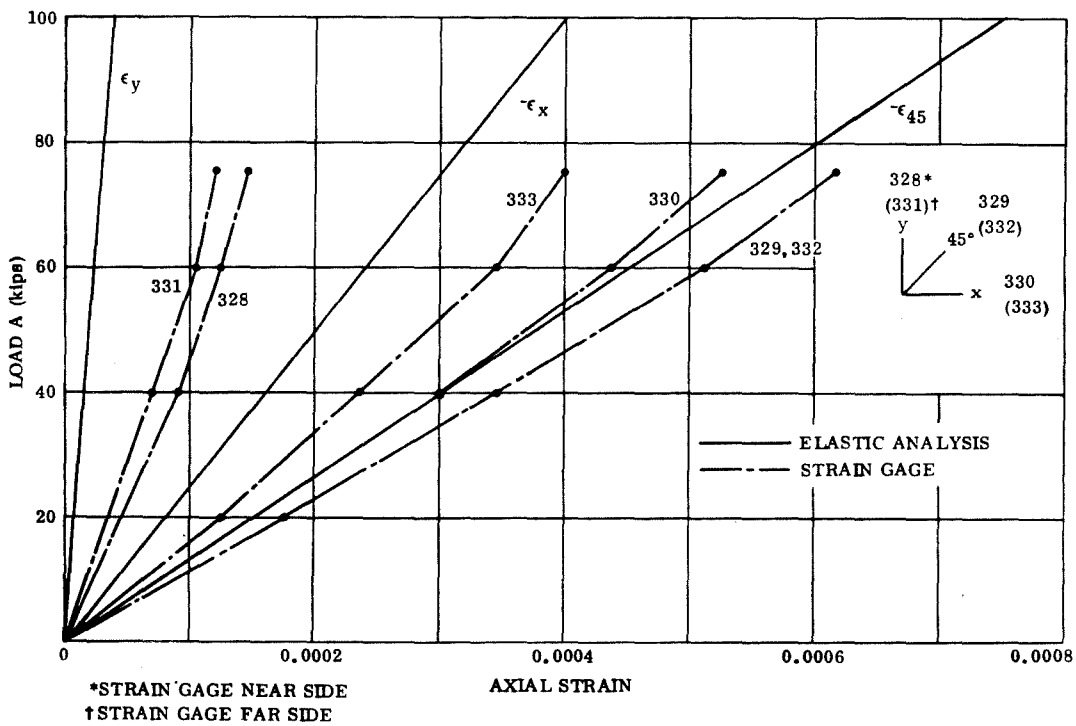

Figure 6-5. Strain Gage Readings and Theoretical Strains at Element 18 of Web for Load Condition 2 (75% of Design Ultimate Load A where Load B is absent)

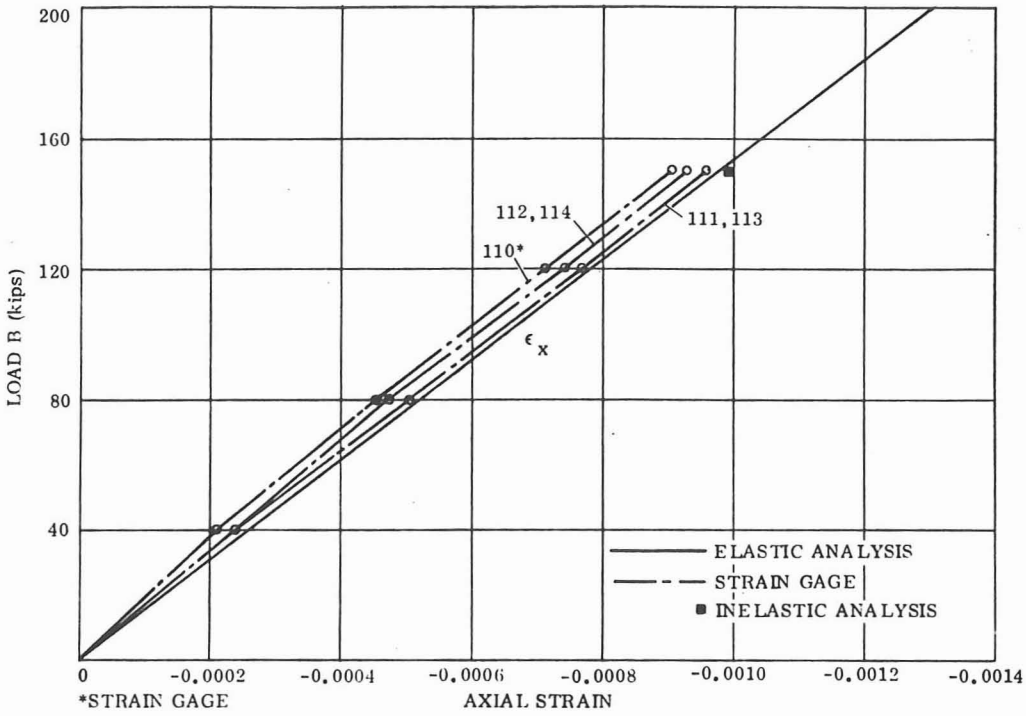

Figure 6-6. Strain Gage Readings and Theoretical Strains at Element 2 of Compression Cap for Load Condition 3 (75% of Design Ultimate Load B where Load A is absent)

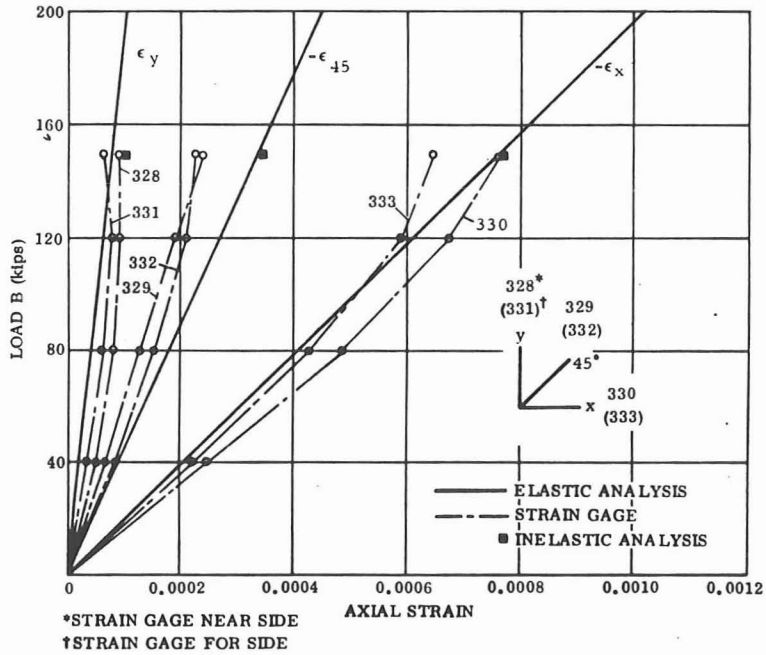

Figure 6-7. Strain Gage Readings and Theoretical Strains at Element 18 of Web for Load Condition 3 (75% of Design Ultimate Load B where Load A is absent)

Table 6-2. Strain Gage/Rosette Analysis versus Elastic/Inelastic Analysis at Element 18 of Web for Load Condition 3 (75% of Design Ultimate Load B where Load A is absent)

STRAIN QUANTITY	STRAIN GAGE (AVE. STRAIN)	ELASTIC ANALYSIS		INELASTIC ANALYSIS	
		STRAIN	DIFFERENCE[2] %	STRAIN	DIFFERENCE[2] %
ϵ_x	-0.000705	-0.000764	8.4	-0.000772	9.5
ϵ_y	0.0000744	0.0000783	5.2	0.0001046	40.6
$\epsilon_{45°}$[1]	-0.000232	-0.000334	44.0	-0.000343	47.8
ϵ_{xy}[1]	0.000166	0.0000184	HIGH	-0.0000193	HIGH
STRESS QUANTITY		STRESS (psi)		STRESS (psi)	
σ_x		-16,360		-16,050	
σ_y		- 3,500		- 4,600	
σ_{xy}		214		- 223	

(1) $\epsilon_{45°} = (1/2)(\epsilon_{xy} + \epsilon_x + \epsilon_y)$

(2) STRAIN DIFFERENCE BETWEEN ANALYSIS AND STRAIN GAGE, ASSUMING STRAIN GAGE VALUE IS CORRECT

SECTION 7

FAILURE ANALYSIS

7.1 WEB SPLICE WELDS

The failure of the stiffened panel occurred during Load Condition 4A at 110% of design ultimate load, where Load A was 490 kN (110,000 lb) and Load B was 980 kN (220,000 lb). The failure mode was the shearing of the web splice spotwelds. The most highly loaded spotwelds are located in Element 12 of Figure 5-1. Accordingly, stresses in Element 12 must be resolved to determine the maximum resultant spotweld load. The procedure followed was to determine the reliability of the finite element stresses in the adjacent Element 13, where strain gages were installed along with gages in adjacent Elements 15 and 21. Figure 7-1 shows plots of strains for Elements 5, 13, and 21 from the inelastic finite element analysis and analysis of the strain gage data. Strains at the center of Element 13 are found from Figure 7-1. Assuming the strain gages are correct, the strains from the inelastic analysis for Element 13 may be corrected by the following factors:

$$C_x = \frac{1550}{1770} = 0.875 \qquad C_{xy} = \frac{530}{580} = 0.913 \qquad C_y = \frac{370}{598} = 0.619$$

For expediency, these correction factors are assumed to be applicable to Element12, where the splice spotwelds are located. Also, stresses σ_x and σ_{xy} from the inelastic analysis for Element 12 are approximately corrected by the factors C_x and C_{xy}, respectively.

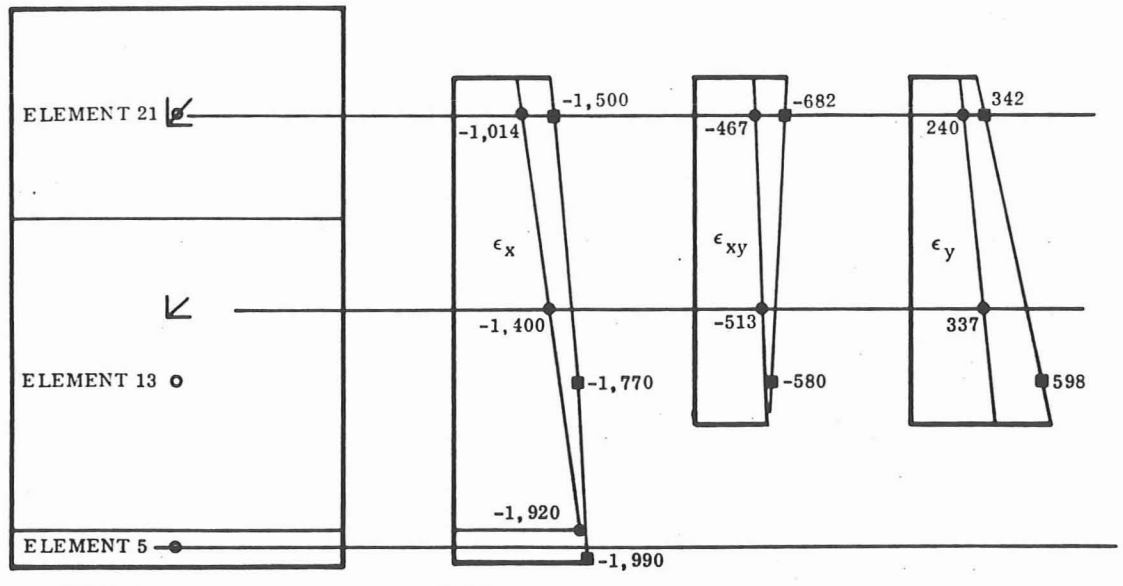

Figure 7-1. Strains in Elements 5 (Compression Cap, 13 (Web), and 21 (Web) for Load Condition 4A (Design Ultimate Load)

From the inelastic finite element analysis, the resulting calculated stresses at ultimate load are:

$$\sigma_x = 0.875(-28,100) = -169 \text{ MPa } (-24.6 \text{ ksi})$$

$$\sigma_{xy} = 0.913(-9,650) = -60.7 \text{ MPa } (-8.8 \text{ ksi})$$

The pitch (p) of the double row of spotwelds is approximately 3.43 cm (1.35 in.), and the web thickness (t) is 0.55 cm (0.22 in.). Consequently, the estimated maximum ultimate loads on the spotwelds are

$$X = \sigma_x pt/2$$

$$= 16.1 \text{ kN } (3612 \text{ lb})$$

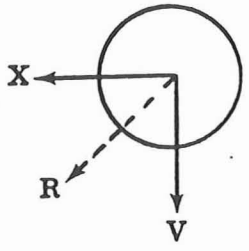

$$V = \sigma_{xy} pt/2$$

$$= 5.6 \text{ kN } (1274 \text{ lb})$$

and the resultant load is

$$R_{ult} = \sqrt{\overline{3612}^2 + \overline{1274}^2} = 17.1 \text{ kN } (3837 \text{ lb})$$

Now, since failure occurred at 110% of ultimate load, the resultant load at failure is

$$R_{failure} = 1.1 \times 3,837 = 18.8 \text{ kN } (4220 \text{ lb})$$

Some very limited testing (Reference 2) indicated the spotwelds in the skin splice had an average value of 4000 pounds, which is in excellent agreement with observed results.

7.2 LOCAL PANEL BUCKLING ANALYSIS

The B/Al stiffened panel is a representative structure for the compression side of a Space Shuttle thrust structure where the maximum stresses in the web are nearly constant over a considerable length. Because of this, tapering the thickness of the stiffened panel web was not considered, although the manner of test loading would permit the thickness to vary. The compression cap cross-sectional area was varied, however, to properly accommodate the buildup of compression load. The buckling

analysis of the stiffened structure focused on the panel and included Elements 10, 18, 26, 34, 42, and 50 as shown in Figure 5-1. Stresses on the panel are shown in the appropriate directions in Figure 7-2.

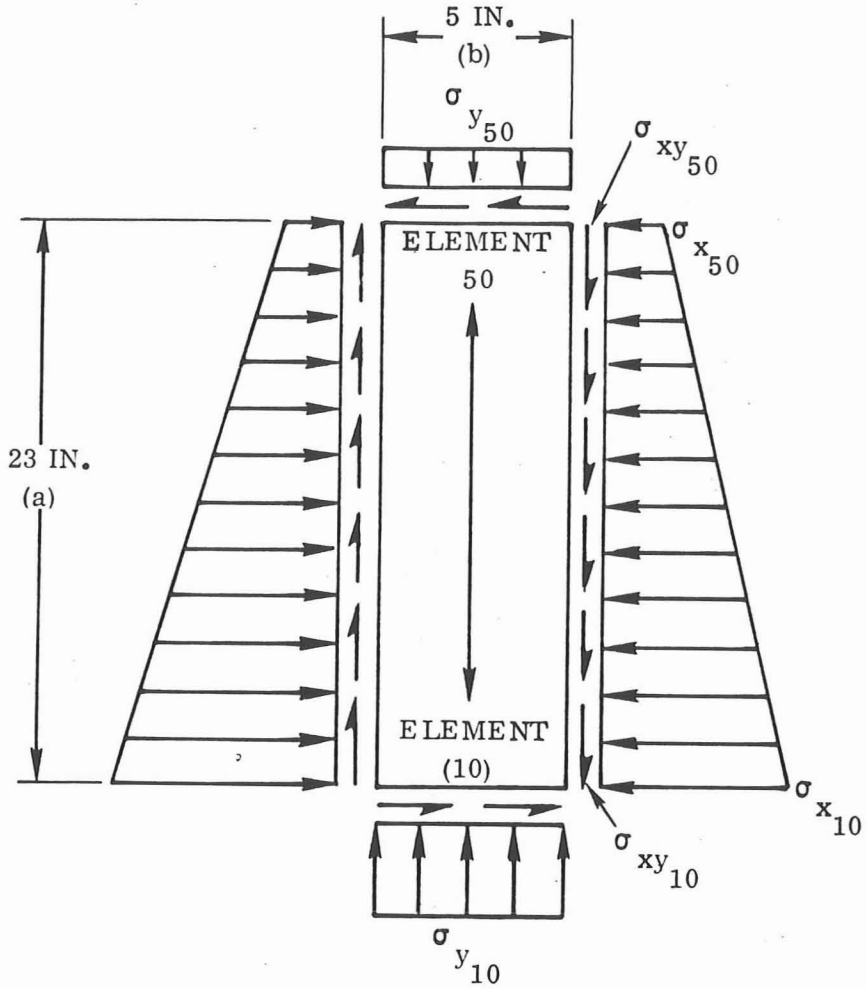

Figure 7-2. Panel of Web with Combined Stresses

The compressive stresses in the x-direction are of sufficient magnitude as to require plasticity corrections for the calculated elastic buckling stress. Consequently, elastic buckling allowables ($\sigma_{x_{cr}}$, $\sigma_{y_{cr}}$ and $\sigma_{xy_{cr}}$) were obtained, and corrected for plasticity effects as necessary. Appropriate interaction curves were then used to establish margins of safety. Since the panels are supported by symmetrical I-section stiffeners, the panels were assumed to be supported in a manner giving an effect midway between that of simply supported and clamped edges.

The stresses from the inelastic finite-element analysis at design ultimate load for the panel in Figure 7-2 are

Element 10		Element 50	
σ_x	= 207 MPa (30.1 ksi)	σ_x	= 51 MPa (7.4 ksi)
σ_y	= 115.1 MPa (16.7 ksi)	σ_y	= 19.3 MPa (2.8 ksi)
σ_{xy}	= 124.8 MPa (13.1 ksi)	σ_{xy}	= 83.4 MPa (12.1 ksi)

7.3 BUCKLING IN THE y-DIRECTION

The appropriate orthotropic elastic buckling equations for compression in the y-direction are (Reference 9, Section 2.2):

Simply supported edges

$$\sigma_{y_{cr}}/\eta = (2\pi^2/b^2t)\left[(D_{xx}D_{yy})^{1/2} + D_{xy} + 2D_{66}\right] \tag{7-1}$$

Clamped edges

$$\sigma_{y_{cr}}/\eta = (\pi^2/b^2t)\left[4.6(D_{xx}D_{yy})^{1/2} + 2.67D_{xy} + 5.33D_{66}\right] \tag{7-2}$$

where the stress is conservatively assumed to be of constant intensity over both edges of the panel.

7.4 BUCKLING IN THE x-DIRECTION

An orthotropic elastic buckling equation for biaxially loaded rectangular plates with simply supported edges is in the form (Reference 9, Section 2.2).

$$\sigma_{x_{cr}}/\eta = \pi^2/b^2t\left\{\frac{D_{xx}m^4(a/b)^4 + 2(D_{xy}+2D_{66})m^2n^2(a/b)^2 + D_{yy}n^4}{m^2(a/b)^2 + \phi n^2}\right\} \tag{7-3}$$

that must be minimized with respect to the number of half waves (m) in the x-direction and the number of half waves (n) in the y-direction. That is, that set of (m,n) values is sought that results in the lowest possible value for the elastic buckling stress $\sigma_{x_{cr}}/\eta$. The term ϕ is defined by the relation

$$\phi = \sigma_y/\sigma_x \tag{7-4}$$

which can be used to include the effect of stress in the y-direction on the elastic buckling stress in the x-direction. However, the value for ϕ is set equal to zero here since interaction curves are used in buckling analysis for combined stress conditions.

7.5 BUCKLING IN SHEAR

The appropriate equations for buckling of an orthotropic plate in shear (Reference 9 Section 2.2) are:

Simply supported edges

$$\sigma_{xy_{cr}} = (4/b^2t)\sqrt{D_{xx}(D_{xy} + 2\,D_{66})}\ \left[11.7 + 0.532\,\theta + 0.938\,\theta^2\right]$$

where

$$\theta = \frac{\sqrt{D_{xx}\,D_{yy}}}{D_{xy} + 2D_{66}} < 1 \tag{7-6}$$

Clamped edges

$$\sigma_{xy_{cr}} = (4/b^2t)\sqrt{D_{xx}(D_{xy} + 2\,D_{66})}\ \left[18.6 + 1.65\,\theta + 1.90\,\theta^2\right] \tag{7-7}$$

By neglecting plasticity effects ($\eta = 1.0$), the elastic flexural stiffness coefficients of Equation 4-4 are found:

$$D_{xx} = D_{yy} = \frac{Et^3}{12\,(1 - \nu_{xy}\,\nu_{yx})} = \frac{25 \times 10^6 \times \overline{0.2176}^2}{12\,(1 - 0.31^2)}$$

$$= 23{,}748 \text{ lb-in}$$

$$D_{xy} = \nu_{yx}\,D_{xx} = 0.31 \times 23{,}748 = 7361 \text{ lb-in.}$$

$$D_{66} = \frac{G_{xy}\,t^3}{12} = \frac{11.6 \times 10^6 \times \overline{0.2176}^3}{12} = 9960 \text{ lb-in}$$

By using the values of the elastic flexural constants D_{ij}, the solutions for Equations 7-1 and 7-2 are found to be:

Simply supported edges

$$\sigma_{y_{cr}}/\eta = 1278 \text{ MPa } (185.2 \text{ ksi})$$

Clamped edges

$$\sigma_{y_{cr}}/\eta = 2276 \text{ MPa } (330.1 \text{ ksi})$$

The average value for the elastic buckling stress in the y-direction is

$$\sigma_{y_{cr}}/\eta = (185,200 + 330,100)/2$$
$$= 1776 \text{ MPa } (257.6 \text{ ksi})$$

By the use of Figure 4-11, curve C, the correction for plasticity results in

$$\sigma_{y_{cr}} \approx 248 \text{ MPa } (36 \text{ ksi})$$

Equation 7-3 with the value for ϕ equal to zero was solved by a minimization computer code, which predicted the lowest critical elastic buckling stress in the x-direction to be

$$\sigma_{x_{cr}}/\eta = 330 \text{ MPa } (47.8 \text{ ksi}) \quad (m = 1, n = 1)$$

for simply supported edges. To modify this buckling stress for an average between simply supported and clamped edge conditions, use was made of Figure 7-3 (Reference 10, Figure 6.2.1.2a). Here $b/a = 5/23 = 0.217$ and $k_c = 4.1$ and 1.1 for clamped and simply supported edge conditions, respectively. The allowable elastic buckling stress in the x direction is approximated by using the average value of k_c [i.e., $k_c = (4.1 + 1.1)/2 = 2.6$] and is given by

$$\sigma_{x_{cr}}/\eta = 2.6 \times 47,800 = 858 \text{ MPa } (124.3 \text{ ksi})$$

The corrected inelastic buckling stress in the x-direction is found by the use of Figure 4-11, curve D, to be

$$\sigma_{x_{cr}} = 259 \text{ MPa } (32.6 \text{ ksi})$$

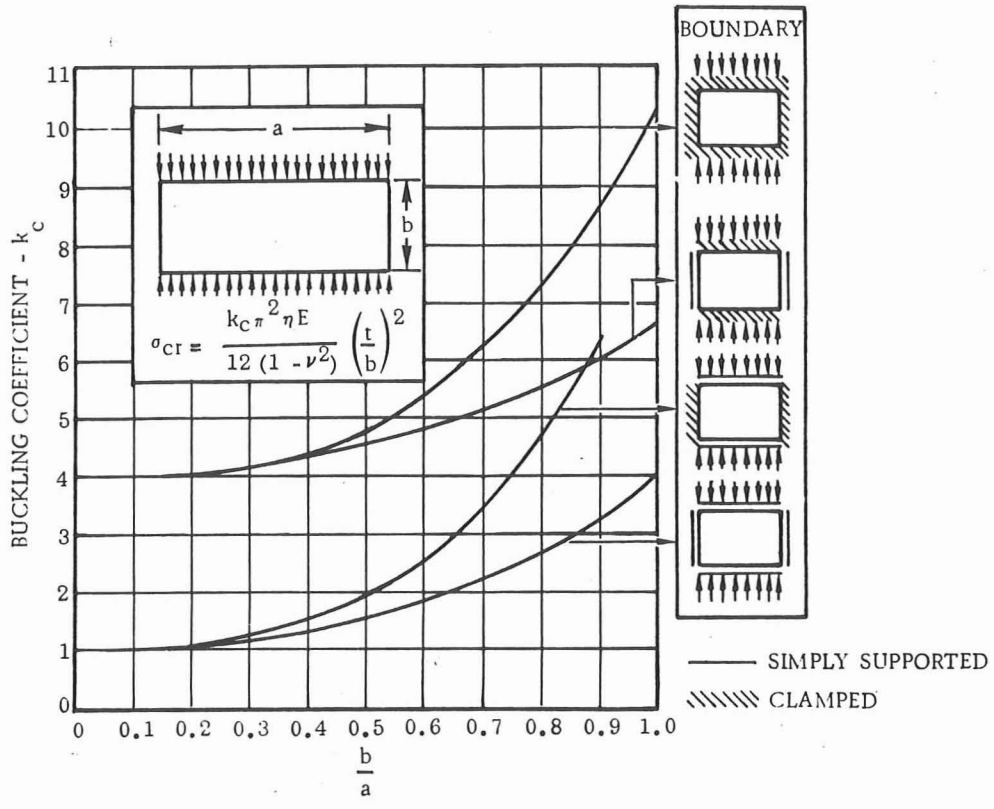

Figure 7-3. Buckling of Short Rectangular Flat Plates in Compression

The solutions of Equations 7-5 and 7-7 for the elastic buckling stress are

Simply supported edges

$$\sigma_{xy_{cr}}/\eta_s = 1662 \text{ MPa (241 ksi)}$$

Clamped edges

$$\sigma_{xy_{cr}}/\eta_s = 2772 \text{ MPa (402 ksi)}$$

The average value is

$$\sigma_{xy_{cr}}/\eta_s = (241,000 + 402,000)/2$$

$$= 2217 \text{ MPa (321.5 ksi)}$$

By the use of Figure 4-10, curve H, it is obvious that the allowable inelastic shear buckling stress is at least equal to 386 MPa (56 ksi), which is the minimum value for F_{su} (see Section 4.1).

7.6 COMBINED STRESS BUCKLING ANALYSIS

The stress ratios for the three stresses acting on the panel are:

$$R_x = \frac{\sigma_x}{\sigma_{x_{cr}}} = \frac{30,070}{32,600} = 0.922$$

$$R_y = \frac{\sigma_y}{\sigma_{y_{cr}}} = \frac{16,680}{36,000} = 0.463$$

$$R_{xy} = \frac{\sigma_{xy}}{\sigma_{xy_{cr}}} = \frac{13,130}{56,000} = 0.234$$

An interaction curve for these stresses is obtained from Reference 10 (Figure 6.2.6.3), and is shown in Figure 7-4 for $R_s = 0.23$. By locating the intersection of R_x and R_y on the graph as shown in Figure 7-4, a small negative margin of safety is indicated for the stability of the panel. However, no buckling of the panels was apparent from the strain gage readings. Accordingly, the inelastic buckling analysis presented here has been conservative.

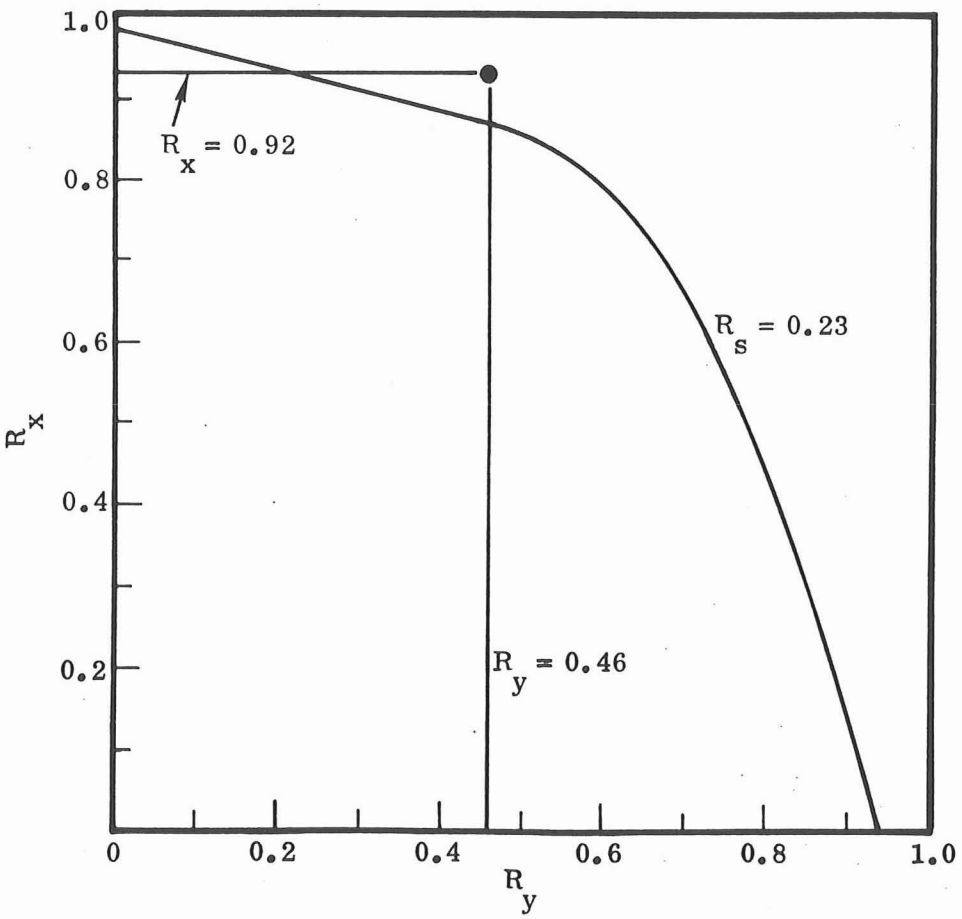

Figure 7-4. Interaction Curve for Simply Supported Flat Plate with a/b = 4 Under Biaxial Compression and Shear ($R_s = 0.23$)

SECTION 8

WEIGHT SAVINGS WITH BORON/ALUMINUM

The all-boron/aluminum (B/Al) composite-stiffened panel, except for the steel tension cap and load introduction fittings, was designed to approximately represent the highly loaded compression side of a B/Al Space Shuttle thrust structure, where the internal stresses were nearly constant. NASA requirements were that the structure be completely stable at ultimate load. Consequently, the weight analysis presented here excludes possible incomplete tension field considerations, although it has been demonstrated and reported in Reference 1 that B/Al has excellent tension field characteristics. The weight study only includes the compression cap, the web, and the outstanding flanges of the stiffeners since they are the elements where B/Al has the most weight savings potential. Accordingly, the alternative use of aluminum and titanium alloy for these elements was considered.

Finite element analyses were performed for a stiffened panel in all-aluminum alloy (2024) and all-titanium alloy (6Al-4V) configurations. Similar assumptions to those used for the B/Al structure were employed. The details of this work are omitted but the significant changes relative to the B/Al design were:

a. Aluminum Alloy (2024)

   1. Compression cap cross-sectional area increased by 50%.

   2. Web thickness increased from 0.55 to 0.7 cm (0.217 to 0.275 in.).

b. Titanium Alloy (6Al-4V)

   1. Compression cap cross-sectional area increased by 50%.

   2. Web thickness decreased from 0.55 to 0.44 cm (0.217 to 0.170 in.).

The all-aluminum and all-titanium alloy shear-resistant stiffened panels were considered to be completely assembled by the use of fasteners. The results of the weight study are shown in Table 8-1 where total weight savings of 34 and 42% were found for B/Al when compared with aluminum alloy and titanium alloy, respectively.

It is thus shown that the boron/aluminum stiffened panel is significantly more efficient than panels made from such conventional materials as aluminum and titanium.

Table 8-1. Weight Savings with Boron/Aluminum

STRUCTURAL ELEMENT	B/Al	2024 Al ALLOY			6Al-4V TITANIUM		
	WT. (LB.)	WT. (LB.)	WT. SAVED (LB.)	% SAVING	WT. (LB.)	WT. SAVED (LB.)	% SAVING
COMPRESSION CAP	11.0	16.5	5.5	33.3	26.4	15.4	58.3
WEB	32.6	41.2	8.6	20.9	40.8	8.2	20.1
FLANGE (VERTICAL STIFFENERS)	2.9	8.8	5.9	67.0	9.2	6.3	68.4
FASTENERS (LWR CAP)	0.6	1.3	0.7	53.8	1.3	0.7	53.8
FASTENERS (VERTICAL STIFFENERS)	—	3.6	3.6	—	3.6	3.6	—
TOTAL	47.1	71.4	24.3	34.0	81.3	34.2	42.1

SECTION 9

CONCLUSIONS

The results from the design, analysis, fabrication, and test of a typical aerospace stiffened panel made from boron/aluminum (B/Al) have been presented. The primary emphasis has been associated with problems concerning the determination of internal stresses in the inelastic web of this structure, which was made from ±45-degree heat-treated B/Al. A method of inelastic analysis for the web material was developed and used to correlate finite element solutions of the structure with strain gage data. Agreement in most instances was satisfactory. The B/Al stiffened panel exceeded design requirements while at the same time representing 34 and 42% weight savings over an all-aluminum and all-titanium design, respectively. This work demonstrates that composite technology has been sufficiently developed to permit the application of B/Al for aerospace structures with a high degree of confidence.

As a result of this program, it is recommended that boron/aluminum be seriously considered in all future trade studies for structural applications where high performance is critical; boron/aluminum has proven to be competitive with conventional materials.

SECTION 10

REFERENCES

1. Miller, M.F., Christian, J.L., and Wennhold, W.F., Design, Manufacture, Development, Test, and Evaluation of Boron/Aluminum Structural Components for Space Shuttle, Volume I, Design and Analysis, GDCA-DB673-006, NASA Contract NAS8-27738, August 1973.

2. Miller, M.F., Christian, J.L., and Wennhold, W.F., Design, Manufacture, Development, Test, and Evaluation of Boron/Aluminum Structural Components for Space Shuttle, Volume II, Materials and Processing, GDCA-DB673-006, NASA Contract NAS8-27738, August 1973.

3. Schaefer, W.H., Christian, J.L., et al, Evaluation of the Structural Behavior of Filament Reinforced Metal Matrix Composites, AFML-TR-69-36, January 1969.

4. Schaefer, W.H., Aluminum-Boron F-106 Engine Access Door Design and Test Evaluation, Convair Aerospace Division Report GDC-ERR-1514, August 1970.

5. Schaefer, W.H., Wennhold, W., et al, Composite Fuselage Development, Convair-San Diego report to General Dynamics, Fort Worth, for Air Force Contract F33615-70-C-1494, 1969.

6. Forest, J.D., et al, Advanced Composite Applications for Spacecraft and Missiles, Volume I — Structural Development, Volume II — Material Development, AFML-TR-71-186, March 1972.

7. Stowell, E.Z., A Unified Theory of Plastic Buckling of Columns and Plates, NACA TN 1556, April 1948.

8. Fedor, R.J. and Ebert, L.J., "A Study of the Effects of Prestrain on the Tensile Properties of Filamentary Composites," Journal of Engineering Materials and Technology, April 1973.

9. Advanced Composites Design Guide, Volume II Analysis, Air Force Materials Laboratory, Advanced Development Division, WPAFB, Ohio, January 1973.

10. General Dynamics' Convair Aerospace, Fort Worth Division, Structures Manual, 1961.